Mineralogy and Petrology (2019) 113:783–801
https://doi.org/10.1007/s00710-019-00686-8

ORIGINAL PAPER

Petrology and geochemistry of mafic dykes of Sylhet traps, Northeastern India, and their Kerguelen plume linkage

Bibhas Sen[1] · Tapan Pal[1] · Kevilhoutuo Theunuo[1]

Received: 30 January 2019 / Accepted: 19 August 2019 / Published online: 9 September 2019

Abstract

We present here a new set of mineralogical and geochemical data from a cluster of east southeast-trending mafic dykes that intrude a lava flow of Sylhet traps. These tholeiitic dykes remained largely unattended in recent petrological and geochemical characterization of the Sylhet traps. This flood basalt province is believed to be a lava outpouring of Kerguelen plume active in the Northeastern India during the Cretaceous time along with that of the Rajmahal traps and Bengal basin. The studied dykes are generally thin (<3 m), high-angled to vertically dipping. They developed chilled margins along their contacts with the host basaltic lava and are apparently product of single magma injections. The dyke rock is porphyritic basalt with phenocrysts of bytwonite with or without Ca-rich augite set largely in subophitic to intergranular (and/or intersertal) groundmass comprising bytownite/labradorite, augite, titano-magnetite and glass. The major oxide and trace element variations in these dykes indicate that the basaltic magma underwent of fractional crystallization with concomitant assimilation. In spite, the immobile trace elements like Na, Zr, Y and rare earths of uncontaminated and little contaminated dyke samples (Nb/La >0.8) show an undoubted plume-derived character with ΔNb >0 (ΔNb indicates the source characteristics of a basalt sample by calculating excess or deficiency in Nb). These elements also led to identifying the possible genetic connection between these dykes and the Kerguelen plume having similar concentrations and variation patterns with the basalts derived from it. However, robust geochemical, geochronological and palaeomagnetic constraints for both the lava flows and the dykes of Sylhet traps are required to understand the genesis and evolution of igneous activity in this little known domain.

Keywords Geochemistry · Mafic dykes · Sylhet traps · Kerguelen plume

Introduction

Dykes and dyke swarms have immense value in understanding mantle-crust evolution and dynamics. In general, dykes are extensional fractures, i.e., opening or tensile-mode fractures (Gudmundsson and Marinoni 2002). Because dykes propagate as magma-filled fractures in a direction perpendicular to minimal principal compressive stress (σ_3), they facilitate in recognizing the episodes of crustal extension during which large quantities of mafic magma are formed and transported from mantle to crust as signatures of mantle plume activity and associated continental break-up (e.g. Halls and Fahrig 1987; Parker et al. 1990; Baer and Heimann 1995; Ernst et al. 1995, 2001; McHone et al. 2005).

One of such mafic dyke swarms is found in ~117 Ma old continental flood basalt province of Sylhet traps in Northeastern India. The Sylhet traps is exposed as four dominant inliers in a narrow (60 km × 40 km) east–west band towards the southern fringe of Shillong Plateau. It predominantly comprises of sub-aerially erupted basaltic lava flows with minor volumes of alkali basalt, rhyolite and acid tuff (Talukdar 1967; Talukdar and Murthy 1971) (Fig. 1a, b and c). The basaltic lava flows of this province have been characterized on geochemical and geochronological aspects in recent years (e.g. Pantulu et al. 1992; Baksi 1995; Kent et al. 2002; Ray et al. 2005; Ghatak and Basu 2011; Islam et al. 2014). Two sections, namely Cherrapunjee –Shella (CH) in central

Editorial handling: F. Stoppa

Electronic supplementary material The online version of this article (https://doi.org/10.1007/s00710-019-00686-8) contains supplementary material, which is available to authorized users.

✉ Bibhas Sen
bibhas.sen@gsi.gov.in; bibhas.sen@gmail.com

[1] Geological Survey of India, Northeastern Region, Shylla Building, Nongrim Hills, Shillong 793003, India

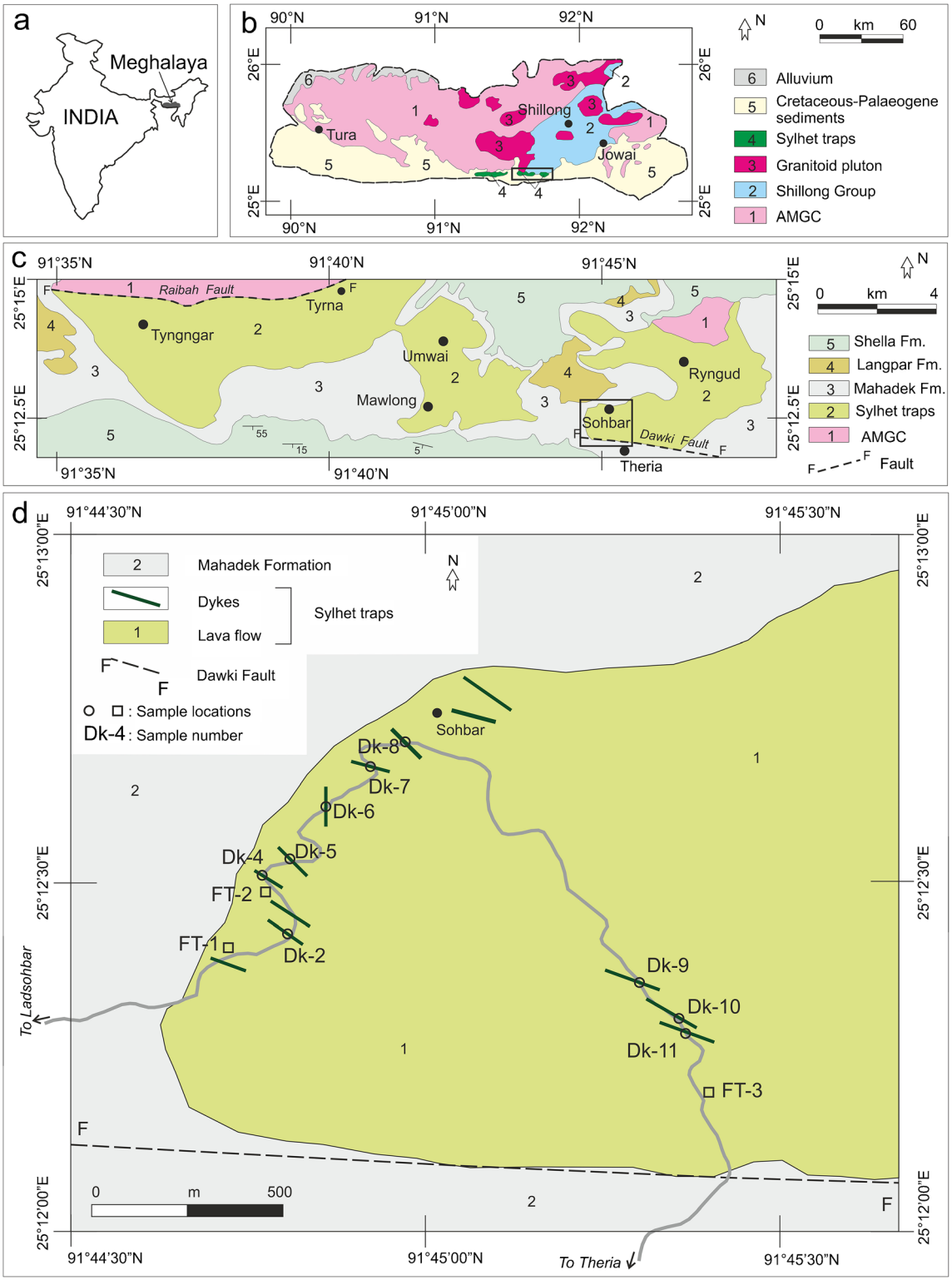

Fig. 1 **a** Location of the state of Meghalaya in northeastern India; **b** Outcrops of Sylhet traps in the southern part of Meghalaya; **c** Studied area of Sylhet traps in and around Sohbar (in black rectangle) (modified after Talukdar and Murthy 1971) along with other inliers of Tynghgar and Mawlong; (B) Sketch geological map of Sohbar area showing the dykes studied along the Sohbar-Theria Road. *Abbreviations*: Fm-Formation, Gp-Group, AMGC-Assam-Meghalaya Gneissic Complex

inlier and Mawsynram-Balat (MB) in western inlier of Sylhet flow basalts, are geochemically well constrained by Ghatak and Basu (2011). Based on geochemistry and geochronology, the Sylhet Traps have been linked with the Rajmahal Traps of

eastern India and both with the Kerguelen Plateau of Indian Ocean (e.g. Storey et al. 1992; Pantulu et al. 1992; Baksi 1995; Basu et al. 2001; Frey et al. 2002, Ray et al. 2005, Ghatak and Basu 2011; Islam et al. 2014). However, the mafic dykes emplaced within Sylhet traps, remained largely unattended on these studies. Mallikarjun Rao (2002) did a preliminary study on the dolerite dykes within the basement gneisses exposed in the western parts of Meghalaya and linked them to the Sylhet volcanism. Likewise, N–S trending mafic dykes emplaced within the Precambrian rocks and exposed in the eastern parts of the Shillong plateau show very close geochemical similarities with the mafic rocks derived from the Kerguelen mantle plume (Srivastava and Sinha 2004). Again, the alkaline-ultramafic complex of Sung, Samchampi, Barpung and Jasra, which are intrusive into the Precambrian rocks of Shillong Plateau and adjoining Mikir hills and, having the similar age of Sylhet traps, have attracted much attention (e.g. Kumar et al. 1996; Veena et al. 1998; Nag et al. 1999; Srivastava et al. 2005; Hoda et al. 1997; Ghatak and Basu 2013).

As mentioned above, although a large number of mafic-ultramafic intrusive bodies of Northeastern India have been characterized, there is a paucity of petrological and geochemical data on the Sylhet dykes. This paper presents the first set of petrochemical data on the Cretaceous mafic dykes emplaced within the lava flows of Sylhet traps. In this work, 12 Sylhet dykes have been studied from the east-central inlier of traps exposed in Sohbar, near Cherrapunjee, Meghalaya state of Northeastern India. Along with their petrographic, geochemical characterization and petrogenetic considerations, we have characterized limited samples of the host basaltic lava flow for comparison. The main objectives of this study are to (i) understand the emplacement dynamics of these dykes and their petrogenetic evolution vis-à-vis that of Sylhet lava flows, and (ii) evaluate their relationship, if any, with the Kerguelen plume activity. We have used a few key trace elements of Sylhet dykes as a clue to their derivation from a plume source and further explored the possibility of Kerguelen hotspot as their plume. Moreover, we have also tried to identify avenues of further research in this largely unexplored Cretaceous flood basalt province.

Geological setting and field relations

Sylhet traps overlie the Precambrian basement of Assam-Meghalaya Gneissic Complex (AMGC) comprising older granite gneiss (~1100 Ma or older) with metapelitic supracrustals and younger granite plutons (~500 Ma) as predominant components (Yin et al. 2010; Kumar et al. 2017). Trap rocks are overlain by Cretaceous-Palaeogene sedimentary sequences (Fig. 1b). The sedimentary sequences have been eroded at places along the E-W fault systems of Dawki while exposing the traps as inliers (Talukdar and Murthy 1971). Three dominant inliers, exposed from west to east, are in Mawsynram-Balat, Cherrapunjee-Shella, and Sohbar-Ryngud area, respectively (Fig. 1c). The central inlier of Cherrapunjee-Shella can be divisible into two distinct sectors of Tynghar-Tyrna (west central) and Mawlong-Umwai (east central). The Sohbar area of Sylhet traps, is a part of eastern inlier of Laitiam-Tyngad (Fig. 1c). It exposes nearly 125 m thick pile of P-type pahoehoe flow of Sylhet traps below the Cretaceous sub-horizontal sedimentary rocks of Mahadek Formation (Sen and Pal 2019). An east-west trending Dawki fault limits the southern extension of Sylhet lava while bringing the overlying sandstones of Mahadek Formation in juxtaposition to it.

In the road-cut of Sohbar-Theria road at least 12 basaltic dykes are exposed (Fig. 1d). In addition, two more basaltic dykes were mapped in the Sohbar village. Geometrical parameters of these dykes are presented in Table 1. All these dykes have an overall trend of ESE-WNW, except dyke Dk-6, which has a N-S orientation. The predominant ESE-azimuth of these dykes are in close conformity with the earlier reported dyke trends ranging from N.75 °–95 °E (Talukdar and Murthy 1971). Considering an overall E-W trend of Sylhet dykes, the local direction of σ_3 during their emplacement was approximately N-S (except for dyke Dk-6) as these dykes do not show any evidence of post-tectonic folding deformation. Presence of dyke oriented at roughly 90 ° to the main strike of the swarm, like Dk-6, is not exceptional. In the areas of crustal fracturing and rifting, occasional abrupt change in the stress field controlling the dyke emplacement might have led to emplacement of few dykes with azimuth high angle to the overall trend of the swarm (e.g., Gudmundsson 1995; Babiker and Gudmundsson 2004). However, the time relation between ENE- dykes and N-dyke is not known as these dykes are traceable only for a limited length, generally ranging from 5 to 10 m.

Most dykes vary in thickness from about few 10s of cm (min. 40 cm in dyke Dk-3) to few hundred cm (max. 350 cm in dyke Dk-9). However, two thickest dykes recorded are Dk-7 (~8.0 m) and Dk-8 (~8.5 m). These dykes generally have very steep (>80 °) to vertical dip (Fig. 2). Dyke rocks are preferable pathways for streamlets as in case of dyke Dk-4 (Fig. 2b).

These mafic dykes that intrude the host pahoehoe basaltic flow are not traceable into or reported from surrounding younger sedimentary sequences indicating their emplacement during Sylhet volcanism. Dykes have developed single set of chilled margins in contact with the host lava flow. These margins, with thickness varying from few centimeters to about 25 cm, show extensive alteration compared to core parts of the dykes. The dykes usually have a few horizontal columnar (cooling) jointed rows, each rows comprising regularly arranged columns that are defined by polygonal fractures of

Table 1 Physical parameters and petrographic characteristics of the dykes and lava flow of Sylhet traps in the study area

Sample	Approximate strike/dip	Approximate thickness (m)	Phenocryst assemblage	Groundmass phases	Groundmass texture
Dk-2	N.125°/90°	1.25	Glm-Ol (1 vol%); Glm-Pl (11 vol%)	Pl, Px, Op, Gl	Sub-ophitic; intergranular and intersertal
Dk-3	N.123°/90°	0.4	–	Not sampled	–
Dk-4	N.122 °/80°	3.0	Ophitic Px (23 vol%), Pl (1 vol%)	Pl, Px, Gl, Op	Sub-ophitic and intergranular; vesicles filled with glassy mass
Dk-5	N.135°/90°	1.2	Glm-Pl (10 vol%)	Pl, Px, Op, Gl	Intergranular, sub-ophitic
Dk-6	N.0°/90°	0.7	Glm-Pl (13 vol%)	Pl, Px, Op, Gl	Intergranular; sub-ophitic
Dk-7	N.105°/90°	8.0	Glm-Px (1 vol%), Pl (14 vol%), Mic. Ol (<1 vol%)	Pl, Px, Op, Gl	Sub-ophitic; intergranular
Dk-8	N.110°/90 °	8.5	Glm-Px (1 vol%), Pl (7 vol%)	Pl, Px, Op, Gl	Intergranular; sub-ophitic
Dk-9	N.110°/90 °	3.5	Glm-Pl (11 vol%)	Pl, Px, Op, Gl	Intergranular, sub-ophitic; amygdular
Dk-10	N.110°/75°	2.0	Glm-Pl (8 vol%); Mic-Ol (<1 vol%)	Pl, Px, Op, Gl	Intergranular, sub-ophitic; amygdular
Dk-11	N.110°/80°	2.0	Pl (3 vol%)	Pl, Px, Op, Gl	Sub-ophitic, intergranular
FT-1	–	–	Ol	Pl, Px, Op, Gl	Intergranular, sub-ophitic; amygdular
FT-2	–	–	Not found	Pl, Px, Op, Gl	Intergranular, sub-ophitic; amygdular
FT-3	–	–	Not found	Pl, Px, Op, Gl	Intergranular, sub-ophitic; amygdular

Abbreviations- Pl: Plagioclase; Px: Clinopyroxene; Ol: Olivine; Op: Opaques; Gl: Glassy material; Glm: Glomerophyric; Mic: Microphenocrystic

similar dimensions. Most of the thinner ones (~3 m across or less) have three columnar rows (e.g. Dk-5 in lower part of Fig. 2a), though somewhat crudely developed in the core parts. The thin dykes are apparently products of single event of magma-injections. In contrast, the thicker dykes (e.g. Dk-8) having 5 or more rows of horizontal columns are interpreted to be due magma injection in several pulses spanning over a few years to hundreds of years (Gudmundsson 1983, 1984, 1995). Petrographic observations also support the episodic nature of melt injection in Dk-8. Other than the cooling joints, dykes do not show any evidence of post-tectonic folding deformation. However, in few cases like Dk-5 and Dk-11, evidences of post-solidification shearing (Fig. 2a) sympathetic to the E-W trending Dawki fault, were observed.

Sample preparation and analytical techniques

Fresh rock samples ($n = 9$) of different dykes were collected from their core portions away from the altered chilled margins. Samples ($n = 3$) of the host flow were collected from different elevations (sample FT-1 from 545 m, FT-2 from 515 m and FT-3 from 450 m above sea level).

For electron probe microanalyser (EPMA) analysis, regular thin sections (46 mm × 27 mm) of the samples were used. For this, thin slices of rock samples were embedded in epoxy, ground and polished, and coated with carbon. For X-ray fluorescence (XRF) analysis, pressed pallets of rock samples were prepared by mixing thoroughly an amount of 4.5 g of homogenized sample (powered to <200 mesh ASTM size) with 0.3 g wax ($C_{18}H_{36}O_2N_2$) as additive binder. The mixture was pressed by applying a 200 kN force to get a uniform disk of 40 mm diameter over boric acid backing in an aluminum cup. For inductively coupled plasma–mass spectrometry (ICP–MS), 0.1 g of <200 mesh size powdered sample was fused with a mixture of 0.15 g lithium tetraborate (flux) and 0.15 g of anhydrous lithium metaborate (flux) in a same Pt crucible. The cold mass was taken into solution with 25 ml of 8% nitric acid and the solution was taken in 250 ml volumetric flask and made the volume up to 250 ml maintaining 4% HNO_3 medium and 10 ppb In.

Chemical analyses of mineral phases were carried out using a Cameca SX 100 EPMA fitted with four wavelength-dispersive spectrometers. The system was operated at an acceleration voltage of 15 keV and a beam current of 15 nA. The electron beam was focused to a ~1 μm for all minerals. The Kα lines were measured for Si, F, K, P, Cl, Fe, Mn, Ti, Ca, Cr, Na, Mg and Al, and the Lα lines for Zr and Ba. Natural mineral references and synthetic standards were used for calibrating the EPMA. These included orthoclase (for K), wollastonite (for Ca and Si), albite (for Na), haematite (for Fe), corundum (for Al), rhodonite (for Mn), apatite (for P), periclase (for Mg), rutile (for Ti), CaF_2 (for F), NaCl (for Cl), $BaSO_4$ (for Ba), Cr_2O_3 (for Cr) and $ZrSiO_4$ (for Zr). The ZAF correction procedure was applied to reduce the data.

A 2.4 kW PANalytical Magix sequential wavelength-dispersive XRF spectrometer was used to determine major and few trace elements. Element/compound concentration of a sample was determined in XRF through calibration (best-fit regression method after application of proper correction coefficients after getting measured under optical parameter settings with proper peak and background timing (where

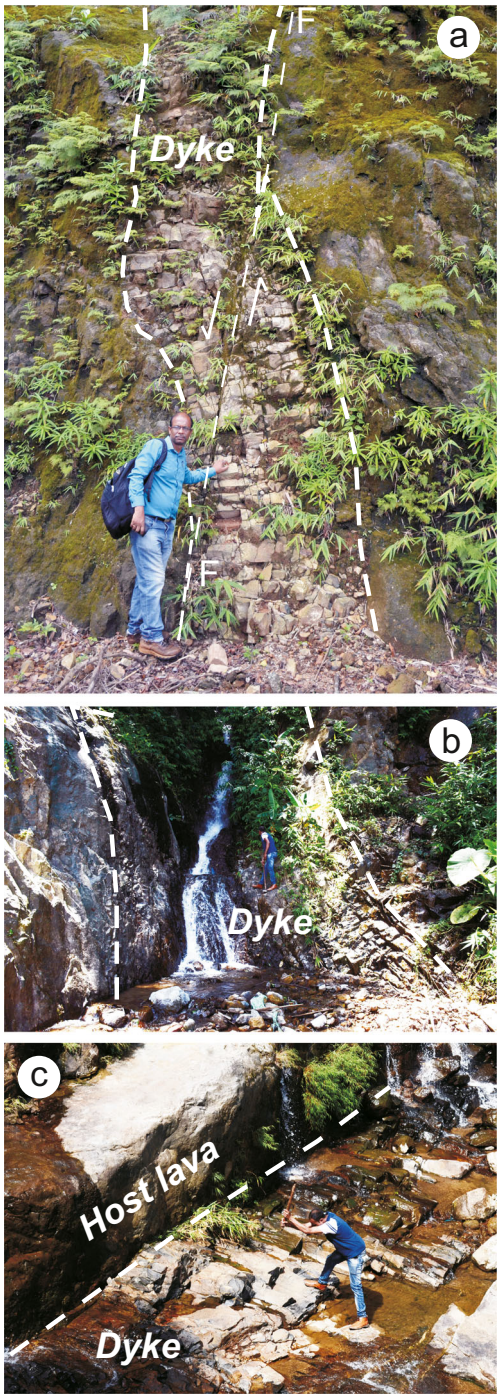

Fig. 2 Field occurrences of mafic dykes showing intrusive relation with the lava flow of Sylhet traps. **a** Sub-vertically dipping dyke, Dk-5, affected by post-emplacement southerly dipping high angle normal fault (marked by line F-F), sympathetic to Dawki fault (viewing direction is towards west). Note the sub-horizontal columns in the footwall; **b** A steeply dipping dyke (Dk-4) along which a streamlet flows; **c** An ~8.5 m thick dyke, Dk-8, with a vertical wall of host lava flow in its northern contact

necessary). The additional set of trace elements (including the rare earth elements, REEs) was analysed using ICP–MS (Varian 820MS). In XRF and ICP-MS analyses, standard reference materials W-2A (Jochum et al. 2015) and GSD-7 (Xie et al. 1985) were run under the same conditions as unknown samples to check analytical accuracy. The analytical uncertainties were found to be ±10% for ICP-MS and 1–3% for XRF analysis. Both of the instruments were set to achieve the lowest concentration of an element (instrumental detection limit) with 95% confidence level (± 2σ standard deviation) eliminating the instrumental drift (drift factor between 0.98 and 1.01). The instrumental detection limits of trace elements detected by these analytical methods are also mentioned in Table 2. The whole-rock geochemical data was processed using GCD-kit v.5.0 software (Janousek et al. 2006).

Results

Petrography

The rocks are porphyritic basalt consisting of glomerophyric aggregate of euhedral plagioclases along with or without subhedral clinopyroxene, set in a groundmass of plagioclase, clinopyroxene, opaque minerals and glass. Plagioclase phenocrysts are present in all the dykes and modally vary from 3 vol% (in Dk-11) to 13 vol% (in Dk-6). However, clinopyroxene is available as phenocryst only in dykes Dk-4, Dk-7 and Dk-8 and vary in proportions from 1 vol% (Dk-7 and Dk-8) and 22 vol% in Dk4. In dykes Dk-2, Dk-7 and Dk-10 olivine, now pseudomorph, occurs as micro-phenocrysts (<1 vol%) (Fig. 3a). In the groundmass, clinopyroxene and plagioclase occur in sub-equal proportion (~40–45 vol%), and opaques and glassy material make up the rest. Very thin apatite needles are found as accessory phase. The commonly observed groundmass textures are sub-ophitic, intergranular and intersertal. The paragenesis of these dykes is typical of tholeiitic basalt. Petrographic characters of the dykes are summarized in Table 1.

The clinopyroxene occurs both as subhedral phenocrysts and anhedral grains in groundmass. The phenocrysts have common size range of 0.5–1.0 mm, whereas the groundmass grains have size of ca. 0.1–0.5 mm. The clinopyroxene phenocrysts invariably occur along with plagioclase in glomerophyric aggregate, as observed in samples of Dk-7 and Dk-8. However, the pyroxene phenocrysts in dyke Dk-4 display ophitic texture by enclosing groundmass plagioclase laths (Fig. 3b). The groundmass grains of pyroxene occur in intergranular to subophitic arrangement with plagioclase laths.

Euhedral to sub-hedral plagioclase generally occurs as fresh prismatic laths and platy grains, respectively, dominating both as phenocryst phase and groundmass constituent. These laths often show simple polysynthetic twinning. The phenocrysts have common size range of 0.5–1.5 mm, whereas the groundmass grains have size of ca. 0.1–0.5 mm. Plagioclase phenocrysts are variably zoned. Often phenocrysts of

Table 2 Representative chemical compositions (EPMA results) and calculated mineral formulae with nominal end-member fractions of the main mineral phases in the dykes under study

Mineral	Clinopyroxene						Plagioclase feldspar						
Analysis#	5	6	12	21–3	22–3	25–3	Analysis#	3	7	9	2–2	2–3	3–3
Dyke	Dk-04	Dk-04	Dk-04	Dk-08	Dk-08	Dk-08	Dyke	Dk-4	Dk-4	Dk-4	Dk-8	Dk-8	Dk-8
Probed phase	Phn (core)	Phn (rim)	Grm	Phn (rim)	Phn (core)	Grm	Probed phase	Grm within ophitic cpx	Phn (core)	Grm	Grm	Phn (core)	Phn (rim)
Oxides (wt%)							Oxides (wt%)						
SiO_2	51.505	51.155	50.81	50.816	51.582	50.818	SiO_2	67.703	67.14	57.915	51.765	49.238	49.478
TiO_2	0.924	0.642	0.927	0.82	0.674	1.23	TiO_2	0.013	0.029	0	0	0.138	0.041
Al_2O_3	2.875	2.74	1.219	1.166	2.219	1.826	Al_2O_3	20.66	20.036	24.219	28.509	30.069	29.662
Cr_2O_3	0.153	0.328	0.008	0.023	0.199	0	Cr_2O_3	0.012	0	0	0	0	0
FeO	7.97	7.474	19.248	18.512	8.277	14.9	FeO	0.315	0.154	0.128	0.68	0.621	0.751
MnO	0.263	0.213	0.369	0.421	0.157	0.367	MnO	0	0	0.021	0	0	0.01
MgO	15.823	16.483	14.369	14.343	16.791	14.985	MgO	0.017	0.043	0	0.041	0	0
CaO	20.581	20.648	13.642	13.179	19.374	15.516	CaO	0.999	0.697	8.437	13.37	15.258	14.992
Na_2O	0.211	0.202	0.23	0.206	0.231	0.136	Na_2O	10.713	11.659	6.4	3.688	2.904	2.961
K_2O	0	0.001	0	0	0	0	K_2O	0.28	0.03	1.789	0.094	0.066	0.074
P_2O_5	0.006	0.018	0.021	0	0	0.022	P_2O_5	0	0	0.06	0.001	0	0.029
BaO	0	0.117	0	0.113	0	0	BaO	0.109	0.078	0.049	0	0	0
ZrO_2	0.036	0	0	0	0.019	0.031	ZrO_2	0	0	0	0	0	0
Total	100.347	100.021	100.842	99.6	99.47	99.829	Total	100.838	99.893	99.046	98.148	98.292	97.998
Calculated mineral formulae (apfu) on the basis of 6O							Calculated mineral formulae (apfu) on the basis of 32O						
Si	1.896	1.883	1.92	1.944	1.908	1.92	Si	11.779	11.802	10.579	9.601	9.183	9.254
Al	0.104	0.117	0.054	0.053	0.092	0.08	Al	4.233	4.148	5.21	6.227	6.604	6.534
Al	0.021	0.002	0	0	0.004	0.001	Ti	0.002	0.004	0	0	0.019	0.006
Ti	0.026	0.018	0.026	0.024	0.019	0.035	Fe^{2+}	0.046	0.023	0.02	0.105	0.097	0.117
Fe^{3+}	0.081	0.066	0.164	0.158	0.045	0.12	Mn	0	0	0.003	0	0	0.002
Cr	0.004	0.01	0	0.001	0.006	0	Mg	0.004	0.011	0	0.011	0	0
Mg	0.868	0.905	0.81	0.818	0.926	0.844	Ba	0.007	0.005	0.004	0	0	0
Fe2+	0.165	0.164	0.444	0.434	0.211	0.35	Ca	0.186	0.131	1.651	2.657	3.049	3.004
Mn	0.008	0.007	0.012	0.014	0.005	0.012	Na	3.614	3.974	2.267	1.326	1.05	1.074
Ca	0.812	0.815	0.552	0.54	0.768	0.628	K	0.062	0.007	0.417	0.022	0.016	0.018
Na	0.015	0.014	0.017	0.015	0.017	0.01							
K	0	0	0	0	0	0							
Σ cations	4	4	4	4	4	4	Σ cations	19.94	20.11	20.155	19.949	20.018	20.009
Calculated mineral fractions (mol%)							Calculated mineral fractions (mol%)						
Wo	41.98	41.642	27.869	27.503	39.281	32.133	Ab	93.6	96.6	52.3	33.1	25.5	26.2
En	44.907	46.253	40.843	41.648	47.368	43.18	An	4.8	3.2	38.1	66.3	74.1	73.3
Fs	13.113	12.105	31.288	30.849	13.351	24.687	Or	1.6	0.2	9.6	0.5	0.4	0.4

Phn Phenocryst, *Grm* Groundmass, *cpx* Clinopyroxene, *Wo* Wollastonite, *En* Enstatite, *Fs* Ferrosilite, *An* Anorthite, *Ab* Albite, *Or* K-feldspar

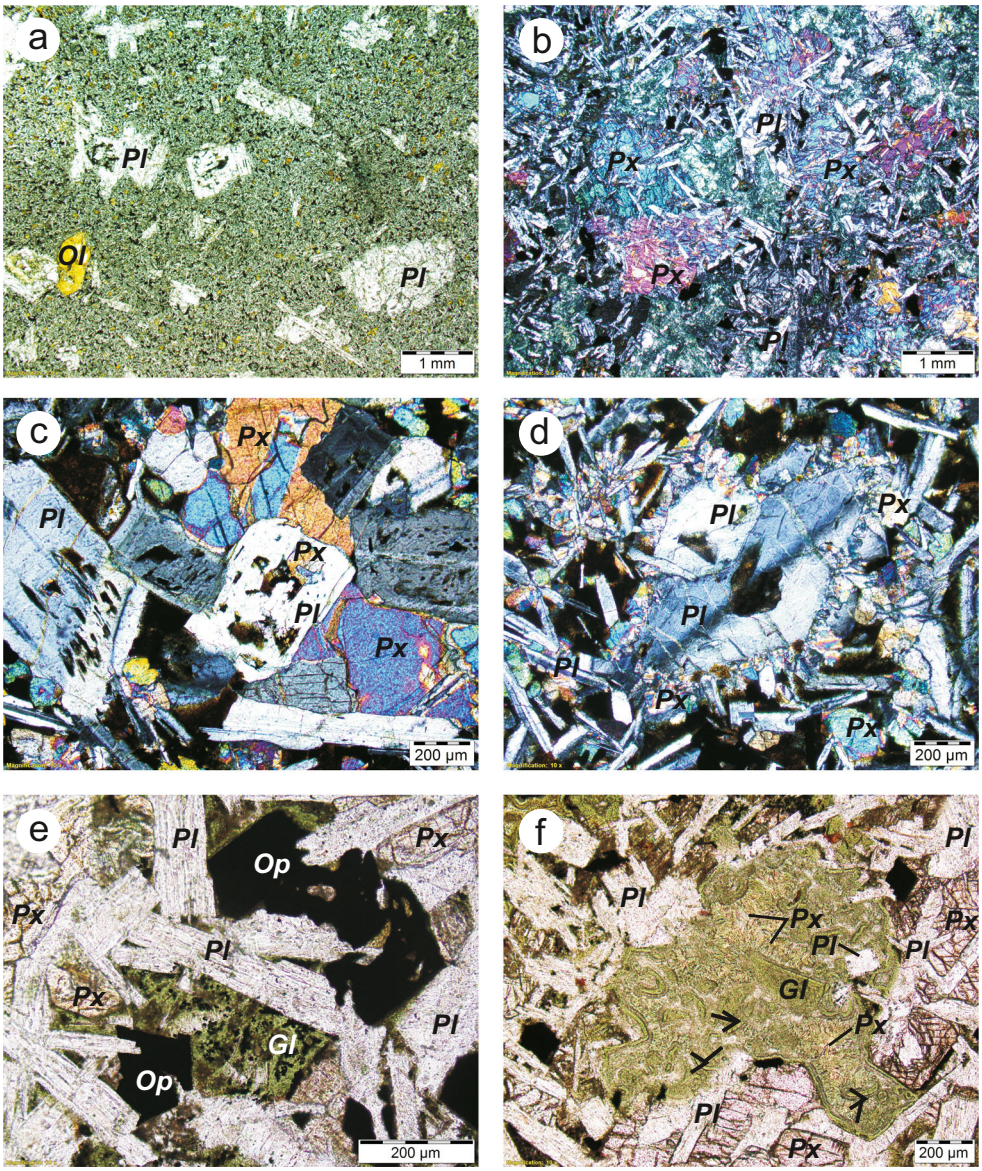

Fig. 3 Salient petrographic characteristics of studied dykes **a** Phenocrysts of plagioclase (in glomerophyric aggregate) and olivine (pseudomorph) set in a very fine-grained groundmass in dyke Dk-2; **b** Ophitic clinopyroxene enclosing laths of plagioclase in dyke Dk-4; **c** Resorbed plagioclase and clinopyroxene as phenocrysts in DK-7; **d** The edges of a plagioclase phenocryst that formed the suitable sites of nucleation of groundmass pyroxene of dyke Dk-8. The phenocryst that later shows tecoblasic overgrowth; **e** Skeletal opaque phases and intergranular drusy glass in groundmass of Dk-4; (f) Altered interstitial glassy mesostasis in dyke Dk-4, with hyalo-colloform selvages (shown with arrow). Microlites of pyroxene and newly formed plagioclase got arrested in the glassy mass. *Abbreviations*: Pl-Plagioclase, Px-Clinopyroxene, Ol-Olivine, Op-Opaque phase, Gl-Glassy material

pyroxene are found in close association with that of plagioclase and makes a glomerophyric aggregate. Resorbed plagioclase phenocrysts, commonly having rounded corners, often develop sieve texture (e.g. in Dk-7; Fig. 3c) as a result of rapid growth enveloping melt due to undercooling (Winter 2014). A few zoned plagioclase phenocrysts show tecoblastic growth with faint pigmenting line representing the remains of assimilated groundmass (Augustithis 1978). On the other hand, blastoid overgrowths of plagioclase, occurring either in phenocryst or groundmass, have embayed margins and enclose completely or partially other pyroxene grains. In the groundmass of Dk-8, it is interesting to observe the elongated pyroxene laths (~0.25 mm long) arranged perpendicular to the crystal surfaces of plagioclase phenocryst. This plagioclase phenocryst, in turn, exhibits tecoblastic growth by engulfing of those pyroxene grains (Fig. 3d). The perpendicular array of groundmass pyroxene grains on the crystal surfaces of plagioclase phenocryst suggests that the latter was suitably undercooled to serve as preferable sites of nucleation for these grains (e.g. Lofgren and Donaldson 1975). The tecoblastic nature of plagioclase phenocryst, in turn, indicates episodic growth of plagioclase phenocryst with core portions representing the composition as inter-telluric phase, whereas, the rim portion (that encloses the pyroxene array) represents post-emplacement crystallization with its growth resulting from its reaction with the melt (now preserved as groundmass) (Augustithis 1978). This petrographic observation may corroborate the episodic nature of melt injection in the dyke, envisaged based on the availability of five or more sets of horizontal columnar joint rows.

Opaque minerals occur invariably in the groundmass. These grains demonstrate different growth stages, having

parallel skeletal grains in very-fine groundmass with intersertal texture to subhedral-anhedral shapes in groundmass with intergranular texture (Fig. 3e).

In some dykes with intersertal texture, glass occurs in the interstitial spaces (as last formed mesostasis in groundmass) and as vesicle-fills (Fig. 3e). Very often glassy mesostatis are occupied by fine, minute, branching dendritic microlites and dusty opaque inclusions. At times, the interstitial glassy mass has devitrified selvages with plagioclase crystals arrested within it, possibly because of quick cooling of dyke melt (Fig. 3f). Glass is generally altered to palagonite, chlorophaeite or clay-like minerals.

The samples of host lava, though show higher degree of alteration compared to the dykes, have more or less similar mineral assemblage and texture. Here, plagioclase occurs as pheonocrysts along with olivine (<5 vol%). Groundmass is sub-ophitic to intergranular with subequal proportion of plagioclase and pyroxene (~45 vol%). Rest of groundmass contains opaque minerals and glassy materials. Amygdales are invariably present in all the lava samples and are filled with zeolite and calcite.

Mineral chemistry

Quantitative microprobe analyses of phenocryst and groundmass mineral phases were done for dykes, Dk-4 and Dk-8. While Dk-8 represented a low MgO (4.79 wt%) sample, Dk-4 has a MgO content as high as 6.6 wt%. The ranges of compositions of pyroxene and plagioclase along with representative BSE images are given in Fig. 4 and the details of cationic calculations are given in the Supplementary Material.

The dykes have Ca-rich augite both in phenocryst and groundmass with composition ranging from $Wo_{42}En_{45}Fs_{13}$ to $Wo_{28}En_{41}Fs_{31}$. The maximum compositional variation in core and rim analyses in phenocryst is noted in Dk-8 from $Wo_{40}En_{47}Fs_{13}$ in core to $Wo_{28}En_{42}Fs_{31}$ in the rim (Fig. 4a and d). Otherwise, there is no perceptible variation in core and rim of the analysed pyroxenes. Even in the ophitic pyroxene grains of Dk-4, the core-rim analyses show hardly any variation (from $Wo_{42}En_{45}Fs_{13}$ to $Wo_{40}En_{47}Fs_{13}$). The groundmass compositions are, however, Ca-poor compared to that of phenocrysts. Here, compositions vary from $Wo_{37}En_{46}Fs_{16}$ to $Wo_{28}En_{41}Fs_{31}$. Even the groundmass pyroxene needles that are arranged perpendicular to blastoid plagioclase in dyke Dk-4 also fall within this composition range. TiO_2 and Al_2O_3 contents in augite are low (0.6–1.2 wt% TiO_2 and 1.2–2.8 wt% Al_2O_3). The equilibration temperatures calculated using the clinopyroxene-liquid geothermometer of Putirka (2008) range from 1221 to 1163 °C in dyke Dk-8 and 1156–1126 °C in Dk-4. The clinopyroxene barometer of Putirka (2008) gave the estimated pressure range between 1.6 and 5.6 kbar in Dk-8 and 0.1 to 4.5 in DK-4, indicating clinopyroxene crystallization during magma ascent or storage in the shallow crust.

In comparison to pyroxenes, feldspars of these dykes exhibit interesting range of compositions (Fig. 4e). In dyke Dk-8, there is hardly any variation between core and rim compositions of bytwonite phenocrysts that range from An_{75} to An_{70}. A core (An_{74})-rim (An_{72}) pair analyses of Dk-8 is shown as an example in Fig. 4e (enlarged). The phenocryst showing blastoid growth (see Figs. 3d and 4b) is labradorite ($An_{75–64}$) with composition. The groundmass laths of the dyke show much increase in albitic component and are labradorite (An_{66} to An_{57}) in composition. Considering anhydrous whole rock composition as liquid in the plagioclase-liquid thermo-barometric calculations (Putirka 2008), the estimated equilibration temperature for Dk-8 ranges from 1214 to 1210 °C and pressure from 0.6 to 4.2 kbar. These assessments are probably on higher side as the water content of melt is not considered here. However, the range of pressure that these feldspar grains crystallized is similar to the estimates we made earlier for clinopyroxene. This possibly indicates that the crystallization of these rock-forming minerals occurred during storage in the upper level crustal chambers as shallow as 20–30 km deep (considering a density of 2.8 g/cm^3) or during magma ascent along the dyke fractures.

The probed grains of plagioclase in Dk-4, in contrast to Dk-8, are surprisingly Na-plagioclase in composition. The plagioclase grains of both phenocryst and groundmass of Dk-4 are albitic in composition ($An_{8–2}$). An andesine (An_{38}) is also identified here as a phenocryst phase. This presence of Na-plagioclase is unusual in the tholeiitic basalt and not understood clearly. The grain is apparently altered with pitted core (Fig. 4c) and may involve post-emplacement albitization by hydrothermal fluids. Other than the above silicates, titanomagnetite is a common oxide phase found in the groundmass of both these dykes and vary in TiO_2 content from 25 to 20 wt% and total FeO from 62 to 65 wt%.

Geochemistry

Generalities

Major oxide data of dykes (Dk-2, −4, −5, −6, −7, −8, −9, −10 and − 11) and trace elements of samples (Dk-2, −4, −6, −8, −10 and − 11) along with host lava samples (FT-1, −2 and − 3) are given in Table 2. Loss on ignition (LOI) values are variable but generally low (0.44–4.26 wt%) in dykes and higher (3.87–6.93 wt%) in the lava samples. Though the effects of alteration on the rocks did not appear that extensive in thin sections, the geochemical indicator of surface alteration, e.g. K_2O/P_2O_5 has wide range of values (0.5 to 1.83) for dykes. The sub-aerial alteration leaches out K easily compared to immobile P, suggesting that the samples with $K_2O/P_2O_5 > 1$ are altered

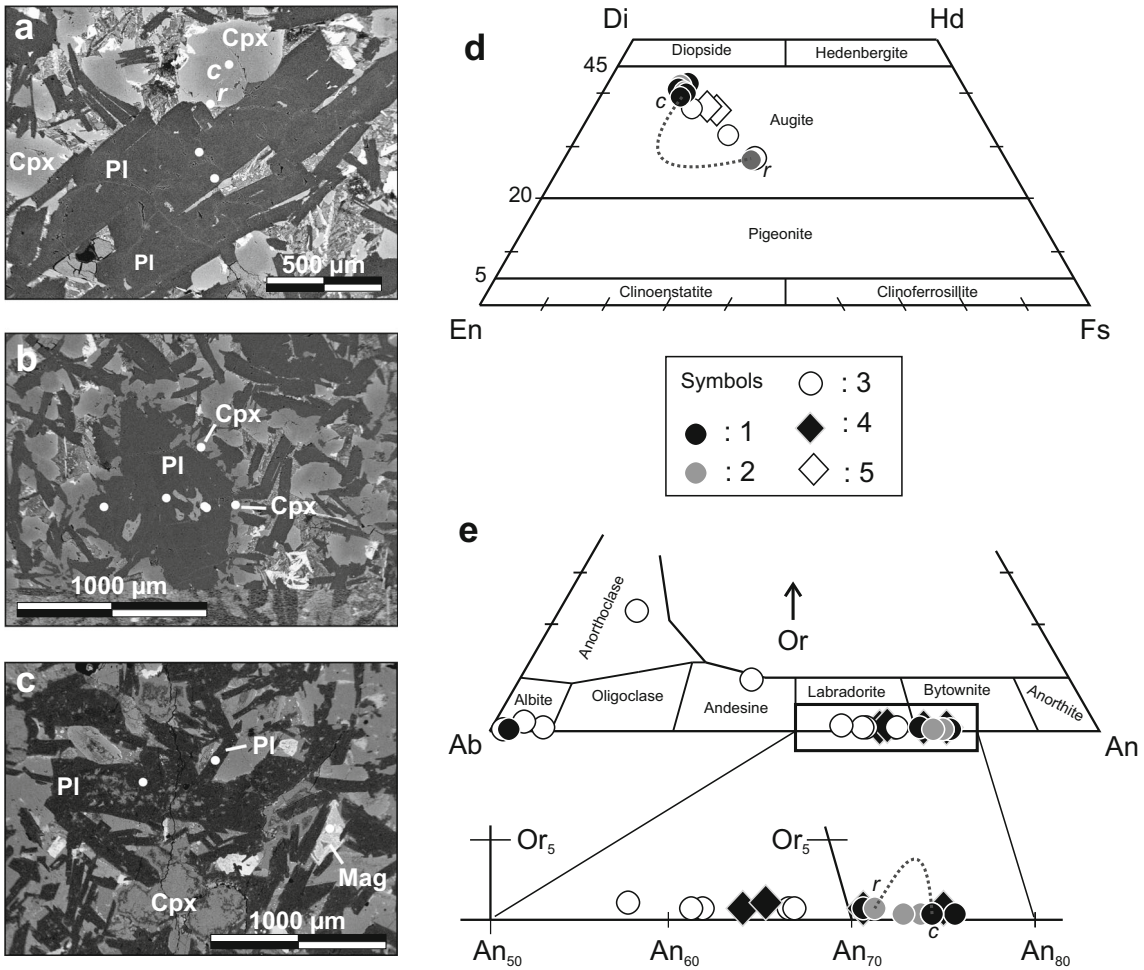

Fig. 4 BSE images and compositional range of pyroxene and plagioclase in the dykes. **a** Images showing points of analyses in phenocrysts of Cpx and Pl in Dk-8; **b** The data points of the blastoid plagioclase phenocryst of Dk-4 with surface perpendicular groundmass Cpx (see Fig. 3, d for corresponding photomicrograph); **c** A plagioclase phenocryst with corroded core portion in Dk-4. **d** Diopside (Di)- Hedenbergite (Hd)- Enstatite (En)- Ferrosillite (Fs) classification diagram for pyroxenes (after Morimoto 1988); **e** Anorthite (An)- Albite (Ab)- Orthoclase (Or) classification diagram of feldspars. A part of the plot is enlarged below. *Symbols*: 1- Phenocryst core (c), 2-Phenocryst rim (r), 3- Groundmass phase, 4: Pl of Dk-4 showing blastoid growth, and 5: Groundmass Cpx perpendicularly arranged to the surface of 4. *Abbreviations*: Pl-Plagioclase, Cpx-Clinopyroxene, Ol-Olivine, Mag-Titano-magnetite

because of sub-aerial weathering since emplacement. Similarly, surface alteration might have affected the concentrations of other mobile elements such as Na, Ca, Ba, Rb, CS, Sr and Pb. Therefore, the present study focuses more on REEs; transition metals such as Cr, Ni, and Sc; and high-field-strength elements (HFSEs) such as Zr, Nb, Ta, Sm, and Hf. The actinide, U and Th have very low concentrations, lesser or close to their detection limits and hence have been sparingly used in this study (Table 3).

Rock classification and tectonic discrimination

In the total-alkali silica (TAS) diagram (Le Bas et al. 1986), the dyke and lava samples plot in the basalt field (Fig. 5a). These samples are shown along with available analyses of Sylhet lavas. As TAS diagram uses mobile elements like Na and K, the validity of this classification of our samples as basalt was further tested. This was done using immobile elements in the Nb/Y versus TiO_2/Y plot of Winchester and Floyd (1977). All our samples plot in the sub-alkaline/tholeiitic basalt in this diagram (Fig. 5b) and this classification is in conformity with the TAS classification. All our samples show a limited spread in these classification plots compared to the published data of Sylhet traps (Ghatak and Basu 2011; Islam et al. 2014).

The basalt geochemistry is popularly known to be diagnostic indicator for discriminating the tectonic setting of origin, when these diagrams use immobile elements and are not used in isolation (Xia and Li 2019). In tectonic discrimination diagram of Zr/Y versus Zr (Pearce and Norry 1979), most of our samples fall in the shared field of 'Within-plate basalt' and 'Mid-Oceanic Ridge basalt' (Fig. 5c). Again, these plot in the field of 'within-tholeiitic basalts and volcanic-arc basalt' at the boundary

Table 3 Major oxides and trace elements of the Sylhet dykes and lava flow of study area

Sample No	Dk-2	Dk-4	Dk-5	Dk-6	Dk-7	Dk-8	Dk-9	Dk-10	Dk-11	FT-1	FT-2	FT-3	W-2A	W-2A	Detection limits
Sample type	Dyke	Dyke	Dyke	Dyke	Dyke	Dyke	Dyke	Dyke	Dyke	Lava flow	Lava flow	Lava flow	Measured value	Reference value	
Oxides (wt%)															
SiO_2	48.62	50.05	49.50	48.33	50.13	49.74	50.07	50.37	50.78	46.08	49.49	48.04	51.87	52.57 ± 0.32	
TiO_2	1.65	1.60	1.86	1.95	2.47	2.26	2.00	2.07	2.24	1.99	1.69	1.78	1.03	1.064 ± 0.01	
Al_2O_3	15.81	14.62	14.66	14.54	14.06	14.33	14.42	14.07	14.34	13.84	13.76	14.74	15.55	15.38 ± 0.09	
Fe_2O_3	13.13	14.00	14.27	14.73	15.11	14.80	14.11	14.65	13.81	13.79	14.38	13.86	10.98	10.80 ± 0.05	
MnO	0.20	0.23	0.22	0.23	0.24	0.24	0.21	0.25	0.25	0.29	0.24	0.25	0.15	0.166 ± 0.003	
MgO	5.98	6.62	5.59	5.83	4.57	4.79	5.67	4.97	5.49	13.45	7.75	7.59	6.31	6.431 ± 0.045	
CaO	12.56	9.86	11.61	12.17	10.63	11.55	11.12	11.19	10.55	8.09	9.74	10.62	10.91	10.91 ± 0.03	
Na_2O	1.80	2.64	2.06	2.01	2.25	1.96	2.02	1.98	2.09	1.71	2.76	2.77	2.27	2.196 ± 0.028	
K_2O	0.10	0.24	0.09	0.07	0.32	0.10	0.20	0.26	0.26	0.62	0.06	0.22	0.69	0.624 ± 0.007	
P_2O_5	0.12	0.14	0.13	0.14	0.22	0.22	0.17	0.16	0.20	0.12	0.13	0.13	0.14	0.136 ± 0.006	
LOI	1.69	4.26	0.98	1.3	0.44	2.63	0.89	1.53	0.6	6.93	4.35	3.87	–	–	
Trace elements (ppm)															
Ba	104	121	88	89	123	123	147	125	136	101	<50	133	175	172.8 ± 1.9	50
Co	47	52	241	93	49	48	52	41	46	50	54	50	45	44.37 ± 0.65	1
Cr	228	128	149	151	87	80	162	126	177	242	174	262	88	92.0 ± 1.6	15
Cu	142	139	173	178	236	204	187	186	223	31	42	104	114	105.9 ± 1.5	1
Ga	28	28	27	26	29	27	37	33	43	26	29	39	22	17.88 ± 0.31	5
Nb	7	7	10	10	15	13	12	11	15	8	8	8	8	7.51 ± 0.15	5
Ni	93	88	100	90	90	77	80	74	86	125	105	121	72	72.0 ± 1.0	2
Pb	14	13	18	5	15	15	5	13	18	12	6	5	8	7.83 ± 0.19	2
Rb	13	15	16	10	18	11	15	14	15	17	11	14	23	20.23 ± 0.27	3
Sc	42	38	41	45	42	36	40	35	34	34	32	43	37	35.86 ± 0.38	3.5
Sr	202	255	177	162	171	188	207	173	164	162	98	185	189	195.4 ± 1.6	5
Th	5	<4	7	<4	4	5	4	4	7	<4	<4	<4	<4	2.179 ± 0.031	4
V	318	323	375	390	420	388	365	388	381	483	362	369	255	265.8 ± 2.9	50
Y	25	22	30	31	36	32	29	31	33	24	25	26	25	21.82 ± 0.33	5
Zn	99	85	131	132	133	116	130	141	136	119	106	102	72	77.7 ± 1.6	10
Zr	97	101	115	115	159	150	125	126	144	88	98	103	101	93.3 ± 1.4	15
Sample No	Dk-2	Dk-4	Dk-5	Dk-6	Dk-7	Dk-8	Dk-9	Dk-10	Dk-11	FT-1	FT-2	FT-3	GSD-7	GSD-7	Detection limits
Sample type	Dyke	Dyke	Dyke	Dyke	Dyke	Dyke	Dyke	Dyke	Dyke	Lava flow	Lava flow	Lava flow	Measured value	Reference value	
Trace elements (ppm)															
La	–	7.72	–	11.39	–	12.76	–	19.18	10.67	7.11	37.51	12.09	46.90	45 ± 6	1
Ce	–	15.90	–	22.10	–	25.17	–	36.36	22.64	14.82	70.85	24.85	77.96	78 ± 7	1
Pr	–	2.49	–	3.34	–	3.70	–	5.10	3.44	2.43	9.14	3.60	9.73	9.6 ± 1.1	0.075
Nd	–	12.82	–	16.25	–	18.08	–	22.37	16.73	11.13	37.12	15.78	37.67	37 ± 6	0.056
Sm	–	3.68	–	4.13	–	4.77	–	5.15	4.53	3.10	7.12	4.15	6.24	6.1 ± 0.5	0.05
Eu	–	1.18	–	1.24	–	1.39	–	1.35	1.37	1.04	1.30	1.09	1.40	1.3 ± 0.2	0.006
Gd	–	3.43	–	3.98	–	4.56	–	4.18	4.62	3.19	6.06	3.87	5.67	5.8 ± 0.8	0.025
Tb	–	0.64	–	0.71	–	0.84	–	0.84	0.85	0.61	0.91	0.67	0.80	0.76 ± 0.14	0.028
Dy	–	4.40	–	4.96	–	5.30	–	5.30	5.48	3.74	4.99	4.58	4.43	4.2 ± 0.14	0.01
Ho	–	0.82	–	0.93	–	1.09	–	0.97	1.03	0.70	0.86	0.83	0.85	0.96 ± 0.21	0.01
Er	–	2.42	–	0.72	–	3.27	–	3.03	2.99	2.20	2.72	2.61	2.40	2.3 ± 0.2	0.01
Tm	–	<0.5	–	<0.5	–	0.51	–	0.50	0.52	<0.5	<0.5	<0.5	<0.5	0.44 ± 0.09	0.5
Yb	–	2.26	–	2.63	–	3.24	–	2.91	3.05	2.35	2.82	2.40	2.63	2.6 ± 0.4	0.003
Lu	–	<0.5	–	<0.5	–	0.53	–	<0.5	<0.5	<0.5	<0.5	<0.5	<0.05	0.39 ± 0.07	0.5

Table 3 (continued)

Hf	–	4.01	–	4.97	–	3.66	–	16.54	3.10	4.88	10.53	4.11	4.18	4.9 ± 1	0.05
Ta	–	<0.2	–	<0.2	–	0.44	–	0.29	0.35	<0.2	<0.2	<0.2	1.37	1.35 ± 0.13	0.2
W	–	7.79	–	<0.5	–	<0.5	–	29.45	6.38	2.63	6.07	<0.5	4.98	5.5 ± 1.0	0.5
Ge	–	1.59	–	1.52	–	1.43	–	1.46	1.20	1.43	1.47	1.51	1.09	1.4 ± 0.4	0.05
Be	–	0.51	–	0.55	–	0.65	–	0.60	0.58	0.44	0.57	0.49	2.67	2.7 ± 0.4	0.03
U	–	<0.5	–	<0.5	–	<0.5	–	0.58	<0.5	<0.5	1.23	<0.5	3.49	3.5 ± 0.5	0.5
Mg#	0.47	0.48	0.44	0.44	0.37	0.39	0.44	0.40	0.44	0.66	0.52	0.52			
Zr/Nb	13.86	14.43	11.50	11.50	10.60	11.54	10.42	11.45	9.60	11.00	12.25	12.88			
La/Nb	–	1.10	–	1.14	–	0.98	–	1.74	0.71	0.89	4.69	1.51			
Nb/La	–	0.91	–	0.88	–	1.02	–	0.57	1.41	1.13	0.21	0.66			
ΔNb	0.06	−0.03	0.14	0.16	0.12	0.06	0.14	0.12	0.17	0.18	0.11	0.08			

W-2A is the standard reference material used in XRF as blank sample. Measured values and reference values with uncertainties at 95% confidence level (Jochum et al. 2015) of W-2A and instrumental detection limits for trace elements are given. Major oxides of dyke samples are recalculated to a total of 100% after subtracting loss on ignition (LOI)

GSD-7 is the certified reference material used in ICP-MS as blank sample. Measured values and reference values with standard deviations (Xie et al. 1985) of GSD-7 are given. Mg# = Mg/(Mg + Fe); ΔNb = 1.74+ log(Nb/Y) -1.92(log Zr/Y) (Fitton et al. 1997)

of 'E-type MORB' field in the ternary tectonic discrimination diagram of Zr/4-2Nb-Y (Meschede 1986) (Fig. 5d). Many studies have found that, in general, the correct identification of tectonic setting is highest for basalts erupted in environments other than 'with-in plate' setting (Wilson 1989; Xia and Li 2019). On the basis of spatial association of these mafic dykes and sub-aerially erupted lava flows of Sylhet traps, 'within-plate' tectonic setting of our samples is quite likely.

Major oxide and trace element relations

Among the relevant immobile oxides/elements, MgO, Ni, and Cr contents of our dykes show ranges of 6.62–4.57 wt%, 100–

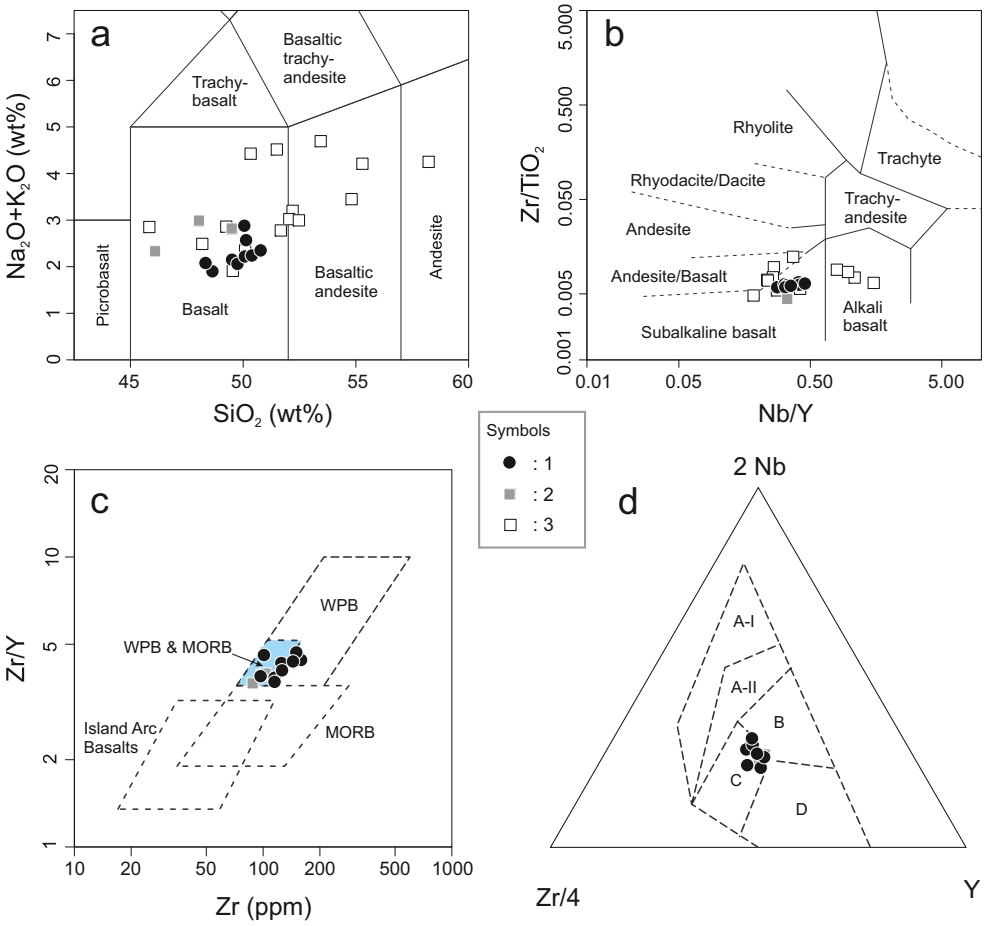

Fig. 5 Geochemical classification plots of the dykes and lava flows of Sylhet traps **a** TAS diagram (enlarged) of Le Bas et al. 1986; **b** Nb/Y versus Zr/TiO_2 plot of Winchester and Floyd (1977); **c** Zr versus Y tectonic plot of Pearce and Norry (1979) [Abbreviations used are WPB: Within-plate basalts, and MORB: Mid-Oceanic Ridge basalts]; **d** Ternary tectonic discrimination diagram of Meschede (1986). Fields are A-I: Within-plate alkali basalts; A-II: Within-plate alkali basalts and within-plate tholeiites; B: E-MORB; C: Within-plate tholeiites and volcanic-arc basalts; D: N-MORB and volcanic-arc basalts. *Symbols*: 1: Dykes (this study); 2: Lava flow (this study); 3: Sylhet trap rocks from previous works (Ghatak and Basu 2011; Islam et al. 2014)

74 ppm, and 226–80 ppm, respectively. TiO_2 contents are 1.6–2.47 wt%. These rocks display no apparent correspondence between MgO and Ni, but distinct positive correlation can be seen between MgO and Cr, MgO and CaO, and Zr and Ti (Fig. 6). The Mg# (=100 × Mg/ (Mg + Fe^{total})) varies from 0.48 (Dk-4) to 0.37 (Dk-7). The low Mg#, Ni and Cr values indicate much evolved geochemical characters of these dykes.

Chondrite-normalized REE patterns of these samples are relatively flat and sub-parallel with $(La/Sm)_N = 2.40–1.35$ and $(La/Yb)_N = 4.73–2.45$ exhibiting mild enrichment of light REEs (Fig. 7a). Dykes have similarity with the pattern of E-type MORB (E-MORB) but somewhat higher concentrations than it. Dykes spread between E-MORB and Ocean Island Basalt (OIB), except for heavier REEs like Tm, Yb and Lu. When compared with the lava flows of Sylhet traps, these dykes show a limited variation in the REE contents and pattern. However, the overall REE pattern of these rocks are more or less similar to the average compositions of lava flows studied by earlier workers in different sections. The dyke rocks have mild Eu anomalies with Eu/Eu* values of 0.89 to 1.02 ($Eu^* = \sqrt{Gd_N.Sm_N}$). The $(La/Yb)_N$ ratios (2.45–4.73) suggesting a transitional stage between E-MORB ($(La/Yb)_N = 1.91$) and OIB ($(La/Yb)_N = 12.29$), though much closer to the former.

To avoid any possible modification in concentration of mobile elements like Na, K, Ca, Ba, Rb, Cs and Sr during weathering and surface alteration of the dyke samples, the primitive-mantle-normalized spider diagram using immobile elements has been explored (Fig. 8b). In this diagram, Th, La and Ce are found to be quite enriched in these dykes. Th shows about fifty to eighty times enrichment in some of these dykes compared to primitive mantle composition (Sun and McDonough 1989). The light REE components like La and Ce also are as high as three times in concentration compared to the E-MORB. Other HFSEs like Nd, Zr and Ti along with Hf show discernible peaks and are higher in concentration compared to the E-MORB. In fact, Hf shows some unusual enrichments in some samples. On the other hand, Nb records mild depletion in some samples, whereas Ta displays marked troughs in almost all the dykes along with P.

Among the mobile elements (not plotted in the spider diagram, Fig. 7b), the concentration of Pb is quite noteworthy (5–18 ppm) and is at least 20–60 times higher in concentration than OIB (3.2 ppm, Sun and McDonough 1989). When compared with the host lava composition (this study) and the average compositions of earlier studied basalts of Sylhet traps (like CH- and MB- sections), the Pb-enrichment of these dykes (5 to 18 ppm; $n = 9$) are much pronounced than the former with their values ranging from 0.64 to 11.7 ppm ($n = 13$; from Ghatak and Basu 2011, and Islam et al. 2014).

Discussion

General remarks

The dykes of Sylhet traps display a range of major and trace element compositions. Generally, the dyke samples have as low MgO (as 4.79 wt%), Mg# (as 0.37), Ni (as 74 ppm), and Cr (as 80 ppm). These values are much lower to the primary

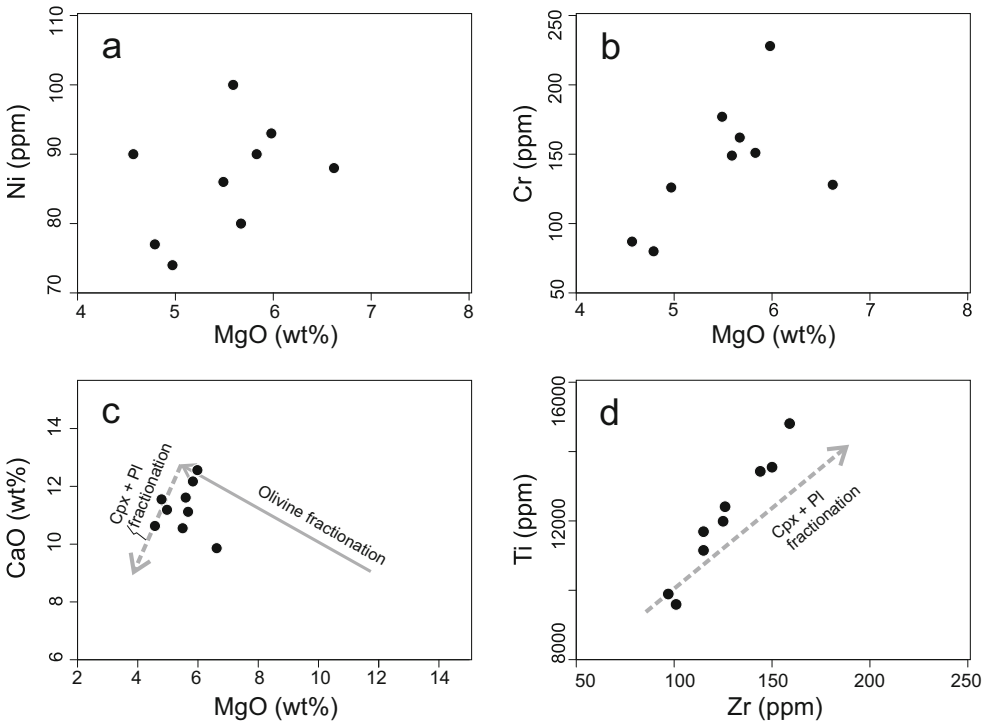

Fig. 6 Binary plots of mafic dykes of Sylhet traps **a** MgO versus Ni; **b** MgO versus Cr; **c** MgO versus Cr; (D) Zr versus Ti

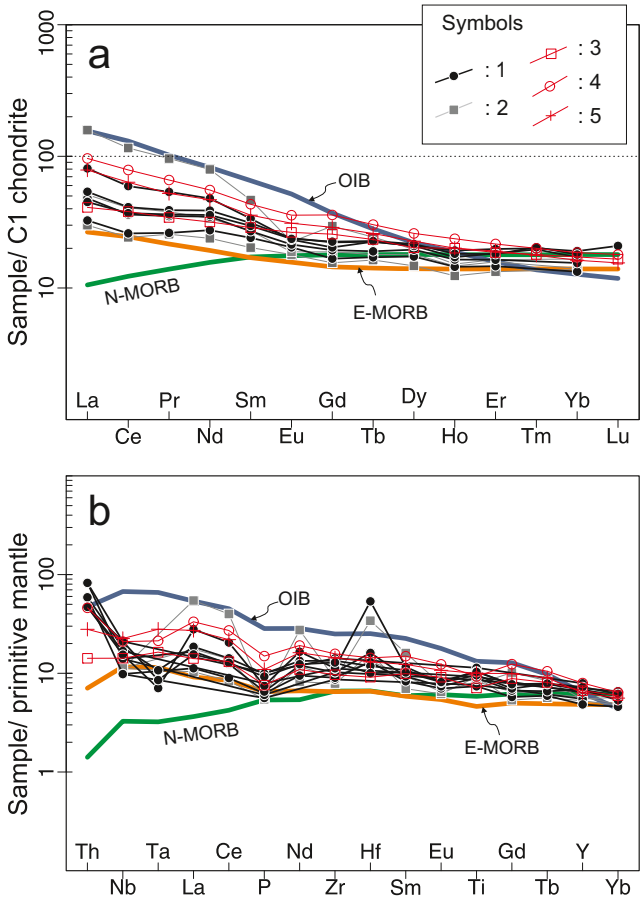

Fig. 7 Spider diagrams of studied dykes and lava flow of Sylhet traps compared with N-MORB, E-MORB and OIB **a** Chondrite-normalized REE pattern, and **b** Immobile element spider diagram of the studied dykes (1) and lava flow (2) along with average values of the reported Sylhet traps lavas in CH-section (3) and MB-section (4) by Ghatak and Basu (2011) and, in Jaflong area (5) by Islam et al. (2014). Normalizing values are C1 chondrite and primitive mantle (Sun and McDonough 1989)

composition generally characterized by Mg# values of >0.7 and high Ni (>400 ppm) and Cr (>1000 ppm) contents (Wilson 1989). This indicates that the parental magnesian magma was evolved during its journey from melt generation to emplacement along the dyke fractures. The resultant geochemical behaviours are suggestive of differentiation processes like fractional crystallization and possibly crustal contamination. However, in spite of having evolved compositions, a few uncontaminated or less contaminated dykes have relevant immobile elements like REEs and HFSEs that are incompatible during fractional crystallization of basaltic magma. We use these key elements to elaborate on the petrogenetic aspects further and explore possible genetic link of these Sylhet dykes with the Kerguelen plume.

Fractional crystallization and contamination

Petrographic features as well as major and trace element variations observed in the studied Sylhet dykes are consistent with fractional crystallization. The positive correlations between MgO and CaO and, MgO and Cr (Fig. 6a, b and c) point toward the fractional crystallization of clinopyroxene from the magma. In addition, the dyke samples show increasing Ti concentration with Zr in the binary plot of Zr versus Ti (Fig. 6d), indicating clinopyroxene and plagioclase as fractionating crystal phases from the already differentiated magma (James et al. 1987). As already noted, petrography suggests that the Sohbar dykes are products of extensive fractional crystallization with clinopyroxene and plagioclase as the leading phenocryst phases with minor participation of olivine in some cases.

The effect of fractional crystallization has been modelled for REEs using spreadsheet program of Esroy and Helvaci (2010) with the most primitive sample (Dk-4) as the parent composition having highest MgO (Mg#) and lowest total REE concentration (Fig. 8a). Considering a Rayleigh fractionation of a crystal assemblage of 5 wt% olivine +20 wt% clinopyroxene +75 wt% plagioclase, a daughter composition of Dk-6 can be achieved with less than 30% crystallization (i.e. 70% fraction of melt remained). However, the light REE (LREE) abundances of the most evolved dyke compositions (e.g., Dk-10) cannot be satisfactorily explained by simple fractionation and call for additional processes involving crustal contamination.

The continental crust is typically low in Ti and highly depleted in Nb and Ta (Barth et al. 2000; Rudnick and Gao 2003). Thus, samples derived from melt contaminated by continental crust are expected to show significant negative Nb-Ta and Hf-Zr (e.g., Tatsumi and Eggins 1995; Zhao and Zhou 2007; Cai et al. 2010; Srivastava et al. 2012; Srivastava et al. 2014). Here, though a few dykes show noticeable Ta and mild Nb depletions, Zr has a somewhat flat pattern while Hf is having well defined peaks (Fig. 7b). In addition, Ti also shows mild peaks for most of these samples. Again, our dykes always plotted in the common field of WPB with either MORB or volcanic arc in the tectonic discrimination diagrams (Fig. 5b and c) and have lower concentrations of important traces like Rb, Th, Zr etc. characteristic of continental flood basalts.

This ‘mixed’ character of trace element concentration of these dykes are quite intriguing and calls for further probing as many continental basalts of the world have ‘mixed’ geochemical characteristics (e.g., Wilson 1989; Wang and Glover 1992; Xia and Li 2019). The contamination by continental crust or lithosphere can impart subduction like signatures (e.g., low Nb, low Ta and low Ti) and lead to the misidentification of contaminated intraplate basalts as ‘arc related’ (e.g. Ernst et al. 2005; Jourdan et al. 2007; Neumann et al. 2011; Xia and Li 2019). We presume that many of our dykes also have undergone lithospheric contamination of various degrees that have resulted in a paradoxical array and concentration of incompatible elements in them.

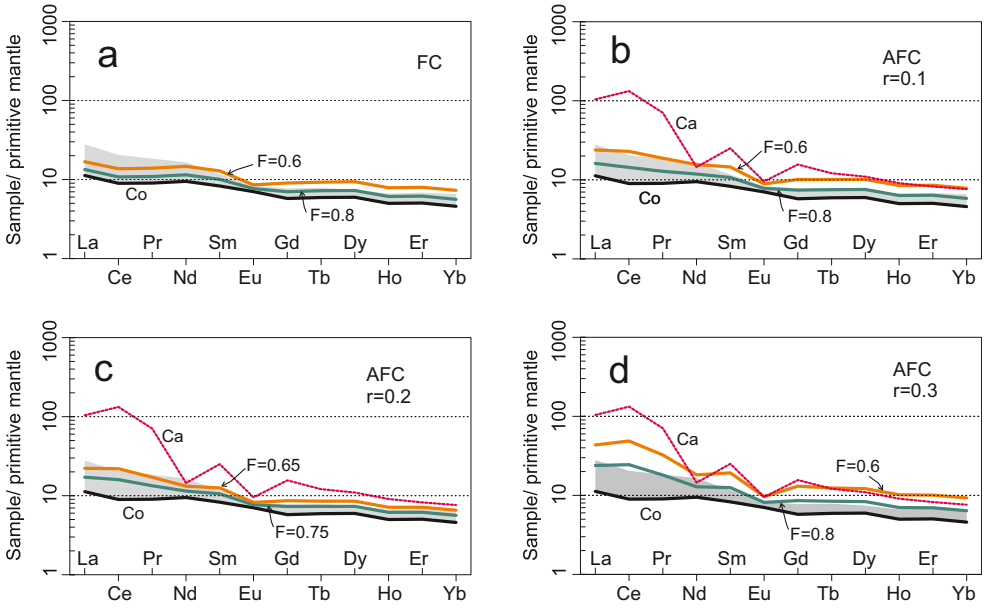

Fig. 8 Primitive mantle normalized REE pattern showing Rayleigh Fractional Crystallization (FC) and Assimilation with concomitant Fractional Crystallization (AFC) model curves for different values (in italics) of F (fraction of melt remaining) with Dk-4 as the parent composition (Co) and a fractionating crystal assemblage of 5% olivine +20% clinopyroxene +75% plagioclase. Ratio of assimilated material to crystallized material, r = 0 for FC (**a**), r = 0.1, 0.2 and 0.3 for AFC (**b-d**). The average composition of granite gneiss ($n = 8$, Kumar et al. 2017) of AMGC is considered as contaminant (Ca). Grey field in each diagram is the compositional field for studied dykes. Primitive mantle values are from Sun and McDonough (1989)

In this regard, Nb/La ratio has often been used to identify the contaminated basalts from the uncontaminated (e.g. Xia and Li 2019). Accordingly, dykes Dk-8 and Dk-11 can be divided as uncontaminated (Nb/La > 1.0) and the others as contaminated (Dk-4, Dk-6 and Dk-10). For the rest (Dk-2, Dk-5, Dk-7 and Dk-9), the degree of contamination is not known due to absence of La values. The uncontaminated samples have slightly higher Nb values of 13–15 ppm compared to the contaminated ones (7–13 ppm).

The selective contamination hypothesis of Sylhet dykes gains further support from the elevated LREE patterns with pronounced Th and Pb abundances in many samples. Typical mantle and crust have Ce/Pb ratios of 25 ± 5 and less than 15, respectively (Furman 2004). Ce/Pb ratios of these dykes range from 2.25 to 4.42 and such Ce/Pb ratios may be caused by fluid metasomatism because the fluid in crust is rich in Pb and almost contains no REE. The existence of fluids usually increases the content of Pb and decreases the Ce/Pb ratios (Cao et al. 2011). The Pb content of some of these dykes are as high as 18 ppm, similar to that of continental crust (17 ppm for upper crust, Rudnick and Gao 2003). Similarly, some of the evolved lava compositions of MB-sections (Ghatak and Basu 2011) and Jaflong (Islam et al. 2014) also have high values as 11.7 and 7.37 ppm, respectively. The possible source of contaminants can be AMGC, the Proterozoic basement of Shillong plateau. This basement complex, over which lavas of Sylhet trap rest, is made of granite gneiss (~1100 Ma or older) with older metapelitic enclaves along with younger (~500 Ma) granite plutons (e.g. Yin et al. 2010; Kumar et al. 2017). The granitic rocks, which possibly walled the shallower sub-volcanic magma chambers, have higher abundances of Th (12–110 ppm) and Pb (40–64 ppm) as well as Ce/Pb ratio as high as 16.5 (Kumar et al. 2017). They are likely to modify the concentrations of large ion lithophile elements and LREE of the mafic melt on assimilation.

To explain the observed range of LREE enrichments, we further assessed the possibility of crustal contamination in these dykes by using the coupled assimilation and fractional crystallization (AFC) model of DePaolo (1981). Considering average granite composition of the AMGC ($n = 8$, Kumar et al. 2017) as contaminant, the degree AFC has been estimated with the same parent composition, Dk-4 (having highest Mg# thought little contaminated, Nb/La = 0.88) to explain the larger span of LREE beyond the consideration of FC model. We assume that same proportion of crystal phases were fractionating from the parent melt while assimilation was underway. Although a lower degree of assimilation (r = 0.1 and r = 0.2; Fig. 8b and c) with varying F values can explain the REE-spread of these dykes with varying success, a LREE-enriched daughter composition akin to Dk-10 (the most contaminated sample with Nb/La = 0.57) can be achieved with ~20% crystallization (i.e., 80% fraction of melt remaining) with r = 0.3 (Fig. 8d) by AFC modelling. Thus, in absence of direct evidences like xenoliths in these dykes, AMGC servers as a suitable proxy composition of the wall rock for crustal contamination model to explain the LREE enrichments in these dykes.

Genetic link between Sylhet dykes and Kerguelen plume

The inference of mantle source compositions of many of the mafic dyke swarms is not straightforward as their compositions are largely affected by bulk assimilation of the continental crustal column through which their magmas ascended (e.g. Cribb and Barton 1996; Halama et al. 2004; Lassen et al. 2004; Mungall 2007; Hari et al. 2018). AFC modelling has also hinted towards involvement of crustal assimilation in some our dykes. In spite, some critical trace elements and their ratios in uncontaminated samples are often used for bracketing the source characteristics as they maintain distinctive values corresponding to different source characteristics. Among these, Zr and Nb are least affected by alteration, and are incompatible during fractional crystallisation of olivine, pyroxene, magnetite and plagioclase from a basaltic magma, and thus provide an indication of the composition of the parental source (Weaver 1991). A plume-derived mafic rocks have high Nb but lower Zr content compared to those from the non-plume sources (Condie 2005). This is explored below in further detail.

In the Nb/Yb versus TiO_2/Yb (Fig. 9a), our dykes and lava basalt plot close to the E-type MORB in the lower limits of deep melting array of OIB. In Fig. 9b and c, some of these samples exhibit concentrations very close to E-MORB in the immobile trace element plots of $(La/Sm)_{PM}$ versus Zr/Nb and Y/Nb versus Zr/Nb. In the latter plot, it can be seen that the dykes plot along the trend of lithospheric contamination of plume-derived magma, as seen in continental flood basalts like the Emeishan large igneous province and pre-90 Ma basaltic lavas from the Kerguelen plume (Xia and Li 2019). The chondrite-normalized REE pattern and concentrations in some dykes are also similar to those E-MORB rather than OIB (Fig. 7a). These patterns are usually thought to be typical of magmas generated by the melting of the asthenospheric upper mantle (e.g. Hooper and Hawkesworth 1993).

Further, the incompatible element ratios like Zr/Nb and La/Nb for the dykes mostly indicate enriched mantle source (EM-I, equivalent of slightly modified bulk earth composition). EM is a common mantle source for basalts and is thought to occur in mantle plumes and as inhomogeneities in the asthenosphere (Condie 2018). The parameter, ΔNb can be used as a fundamental source characteristic, which is insensitive to the effects of variable degrees of mantle melting, source depletion through melt extraction, crustal contamination of the magmas, or subsequent alteration (Fitton et al. 1997). This is often used to distinguish between plume and non-plume sources (e.g. Baksi 2001; Condie 2005). The values of ΔNb [= 1.74+ log(Nb/Y) -1.92(log Zr/Y); Fitton et al. 1997] for most of these dykes are >0 and can be considered to have a 'plume source' including that of Dk-4 with ΔNb = (−)0.03.

The continental flood volcanism of Sylhet traps and adjoining Bengal basin and Rajmahal traps have been genetically related with the break-up of eastern Gondwana, i.e., separation of India, Australia and Antarctica, and the formation of Kerguelen plateau basalts by plume upwelling in early mid-Cretaceous (Storey et al. 1992; Frey et al. 2002; Ghatak and Basu 2011). With time, the plume-derived magmatism changed the tectonic setting from a rifted continental margin (113–118 Ma), to being located within a young, widening ocean (118–40 Ma), to formation of the southeast Indian Ridge (40–30 Ma). Finally, magmatism took place in an oceanic intraplate setting (~30 Ma to present), as the southeast Indian Ridge gradually migrated away from the Kerguelen hotspot (Gautier et al. 1990; Mattielli et al. 2002; Xia and Li 2019).

The pre-90 Ma (~120–90 Ma) magmatic products of Kerguelen plume and other likely Kerguelen-plume related rocks (Burnbury basalts, Naturaliste Plateau, and Rajmahal-Sylhet traps) have a definite set of incompatible elemental and isotopic characters that is different from the Indian MORB composition. These Kerguelen basaltic products have low Nb/La ratios (1.20–0.55; Xia and Li 2019) and extreme Sr-Nd isotopic compositions to reflect a continental lithospheric influence such as in the Bunbury basalts (Frey et al. 1996), Rajmahal basalts (Kent et al. 1997), Naturaliste Plateau and ODP Site 738 (Storey et al. 1992; Mahoney et al. 1995) and define sub-parallel trends extending below the Icelandic array (Neal et al. 2002). Like the lavas of Sylhet traps, the incompatible ratios like Zr/Y, Nb/Y of the studied dykes fall in the same array as that of the Naturaliste plateau, Burnbury basalts and the Site 738 on the Kerguelen Plateau (Fig. 9d). In this plot, our dykes spread between the average basalt compositions of CH- and MB-basalts of Sylhet traps reported by Ghatak and Basu (2011). The CH-section basalts are geochemically similar to those of the least contaminated Rajmahal Group I basalts (Kent et al. 1997). In comparison to the least contaminated Burnbury basalts and other Kerguelen plateau lavas, MB-section basalts are similar to those of Rajmahal Group II (Kent et al. 1997) and showed the distinct evidence of mixing between the Kerguelen plume end member and a lower crustal end member (Ghatak and Basu 2011).

The chondrite-normalized REE patterns of our dykes are compared with that the basalts of Naturaliste Plateau and Site 738 (in Fig. 9e) as the former plot over the compositional fields of these Kerguelen-plume derived lavas in Zr/Y versus Nb/Y diagram (Fig. 9d). It can be seen the Sylhet dykes occupy somewhat intermediate position between the primitive compositions of Naturaliste Plateau and evolved signatures of Site 738 (Fig. 9e). However, the higher concentrations of REE with elevated LREE pattern and mild negative Eu anomaly in the Sylhet dykes are quite different from the flat REE pattern of

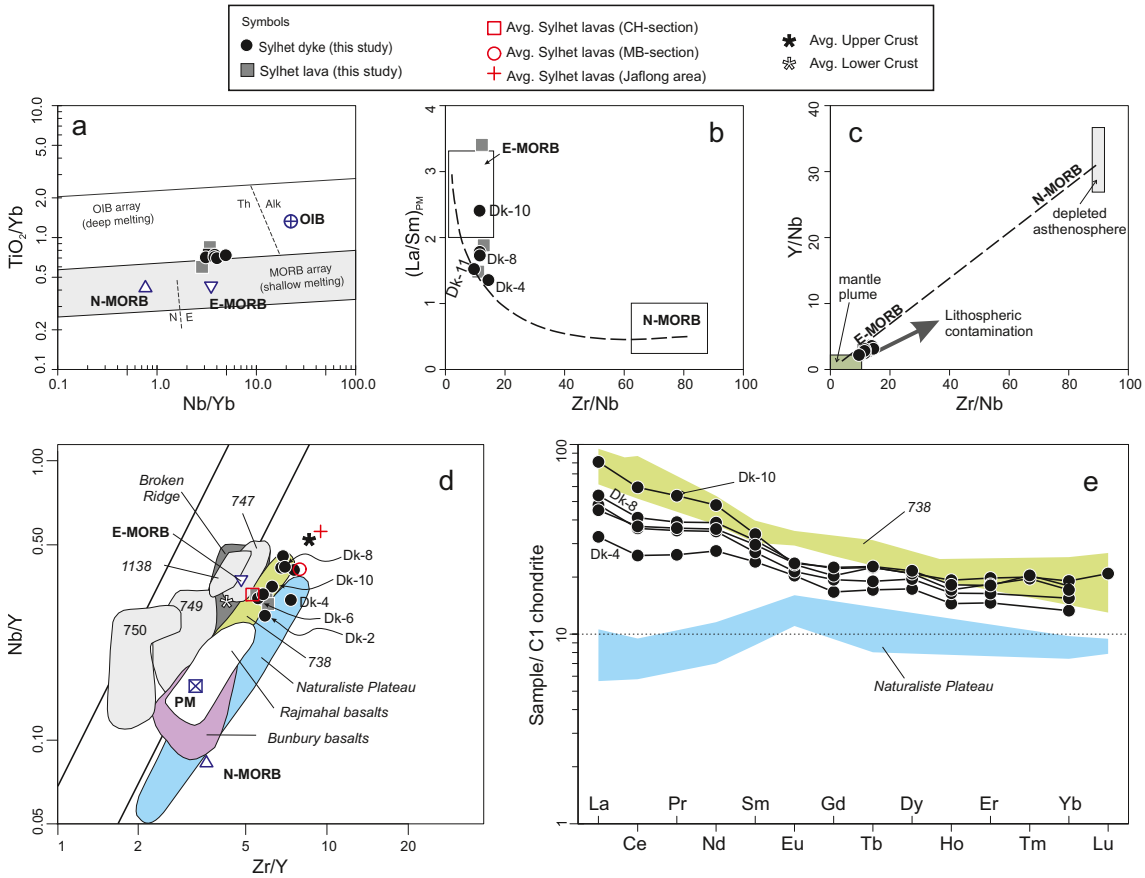

Fig. 9 **a** TiO_2/Yb versus Nb/Yb; **b** $(La/Sm)_{PM}$ (normalized to primitive mantle: Sun and McDonough 1989) versus Zr/Nb; **c** Y/Nb versus Zr/Nb (**b** and **c** are modified after Xia and Li 2019); **d** Nb/Y versus Zr/Y diagrams of the Sylhet dykes and lava flow showing their closeness to E-MORB composition. For comparison, average lava compositions of Sylhet Traps from CH- and MB-sections (Ghatak and Basu 2011) and Jaflong area (Islam et al. 2014) are also plotted on the background compositional fields of Rajmahal basalts, Bunbury basalts, and lavas of South and Central Kerguelen Plateau ODP sites 747, 749, 750, 1136, 1138, 1141 and 1142 related to the Kerguelen Plume (after Neal et al. 2002; Ghatak and Basu 2013). The Icelandic lava data (see Fitton et al. 1997) fall between the parallel lines, but MORB and continental crust lie below the lower line. **e** Chondrite-normalized REE patterns of Sylhet dykes vis-à-vis the basalts of Naturaliste Plateau (except sample SDP264-15CC) and ODP site 738 (data from Storey et al. 1992; Mahoney et al. 1995). Values of C1 chondrite, Primitive mantle (PM), N-MORB, E-MORB and OIB are from Sun and McDonough (1989), and average continental crust compositions are from Weaver and Turney (1984) and Rudnik and Fountain (1995)

Naturaliste Plateau. Closer resemblance of these dykes can be noticed with the pattern of Site 738 lavas in terms of fractionated pattern and abundances of the REEs. Dyke Dk-8 with $(La/Nb)_{PM}$ value of 1.8, which is quite near to the highest $(La/Nb)_{PM}$ values of ~2 of the Site 738 basalts (Neal et al. 2002). Basalts of Site 738 are considered to the most contaminated composition of Kerguelen plume and envisaged to bear the signatures of shallow-level incorporation of continental lithosphere either in the head of the early Kerguelen plume or in plume-derived magma (Mahoney et al. 1995; Neal et al. 2002). However, overall lower REE content of a few of these dykes indicate the depleted nature of their basaltic magma than the melts of Site 738 on Kerguelen Plateau, though much evolved compared to that of Naturaliste Plateau. Thus, the elevated REE budget of the most primitive, uncontaminated or little contaminated dyke compositions of Sylhet traps may be due to inherent enriched character of the melt generated by the Kerguelen hotspot during its position below the Northeast Indian craton at around 117 Ma and the interaction of plume-driven melt with continental lithosphere. The magma was further evolved by fractional crystallization and assimilation in crustal magma chambers and during passage through the dyke fractures puncturing the Precambrian gneissic complex.

Conclusions

Mafic dyke swarms provide information on 'the pulse of the Earth' beyond that is related to oceanic crust generation in the mid-ocean ridge and record the rhythm of intraplate mantle melting events (Ernst and Buchan 1997; Bleeker 2004; Ernst et al. 2010). In this study, we carried out petrographic,

mineralogical and geochemical characterization of a suite of ENE- trending mafic dykes emplaced within the Sylhet traps. These basaltic dykes are apparently product of single magma injection post-dating the extrusion of host lava. The dyke rocks are tholeiitic basalt with bytownite and Ca-rich augite making the predominant phenocrystic phases set in a groundmass of bytwonite/labradorite, relatively Ca-poor augite, titano-magnetite and glass. Thermo-barometric estimations give the crystal-melt equilibrium temperature of ~1150 °C but with a wide range of pressure from ~0.5 to 5.5 kbar corresponding to crystallization during either storage in the crustal level as shallow as 25 km or magma ascent along the dyke fractures.

Petrographical evidences and elemental relations suggest that fractional crystallization was variably responsible for petrological evolution of these dykes. The Nb/La ratio (<1.0) further suggest that some dykes were contaminated by lithospheric components. The REE spread of the dykes can be modelled with Rayleigh fractional crystallization and concomitant shallow-level crustal contamination by the granite/granite gneiss wall rock. Moreover, some of these dykes were possibly affected by fluid metasomatism. However, the issue of albitization, as observed in microprobe analyses of Dk-4, requires further study.

In spite of having evolved compositions, close similarity in the incompatible elemental ratios and characters of the uncontaminated (Nb/La > 1.0) or little contaminated dykes (0.8 < Nb/La < 1.0) with that of Kerguelen Plateau basalts suggest that the Kerguelen plume as a source for these dykes. This inference is in conformity with the earlier works on Sylhet traps, Rajmahal traps and volcanic rocks of Bengal basin (Pantulu et al. 1992; Baksi 1995; Kent et al. 2002; Ray et al. 2005; Ghatak and Basu 2011).

Though Rajmahal traps have received much attention these studies since 1990s, Sylhet traps has remained largely ignored in these multi-disciplinary works except for some recent studies on the lava flows of western and west-central inliers (Ghatak and Basu 2011; Islam et al. 2014). Even in these recent studies, the Sylhet dykes remained grossly overlooked. This study fills this gap and presented new sets of field, petrographic and geochemical data. However, the dykes of other parts of Sylhet traps continue to be unattended in terms of petrological, geochemical, palaeomagnetic and geochronological/isotopic data. In fact, palaeomagnetic data is not available in Sylhet traps, even for the lava flows! Moreover, in some sectors of Sylhet traps, the lava flows need to be characterized using multiple parameters with an aim to erect a unified stratigraphy for the entire province that is valid beyond the physical boundaries of these inliers. Though the studied dykes are intrusive within the pahoehoe lava of east-central inlier, the search for feeder dykes in this flood basalt province will be interesting topic of research. Finding out the physical evidence of dyke spreading like a flow with a 'T'-like exposure may be difficult in this wettest part of the globe characterized by development of thick soil profile and dense vegetation. However, multidisciplinary data will definitely help in narrowing down a set of dykes as feeders, as done in other volcanic provinces like Deccan traps (e.g. Bondre et al. 2006; Vanderkluysen et al. 2011). Robust geochemical, isotopic abundances, geochronological and palaeomagnetic measurements on carefully measured sections and selected samples are required to constrain the petrogenetic evolution of the mafic dykes vis-à-vis the lava flows from this domain.

Acknowledgements Authors are thankful to Mulkh Raj Jarngal, Additional Director General and Head, Geological Survey of India, North Eastern Region, Shillong for providing administrative support to carry out this work. We appreciate efforts of Chinchu Sv (in the EPMA laboratory, Faridabad), Debasis Banerjee (in the XRF laboratory, Chemical Division, Shillong), and Anindya Das (in the ICP–MS laboratory, Central Chemical Division, Kolkata) of the Geological Survey of India, for providing help in or analyzing our samples. Discussions with Amitava Kundu, Sujit Tripathy and Siva Shankar Kambhampati were fruitful. We also thank two anonymous reviewers, handling Associate Editor Francesco Stoppa and Editor-in-Chief Lutz Nasdala for their constructive comments that immensely improved the manuscript.

References

Augustithis SS (1978) Atlas of the textural patterns of basalts and their genetic significance. Elsevier Scientific Publishing Co., Amsterdam

Babiker M, Gudmundsson A (2004) Geometry, structure and emplacement of mafic dykes in the Red Sea Hills, Sudan. J African Earth Sc 38:279–292

Baer G, Heimann A (eds) (1995) Physics and Chemistry of dykes. Balkema, Rotterdam

Baksi AK (1995) Petrogenesis and timing of volcanism in the Rajmahal flood basalt province, northeast India. Chem Geol 121:73–90

Baksi AK (2001) Search for a deep mantle component in mafic lava using a Nb–Y–Zr plot. Can J Earth Sci 38:813–824

Barth MG, McDonough WF, Rudnick RL (2000) Tracking the budget of Nb and ta in the continental crust. Chem Geol 165(3–4):197–213

Basu AR, Weaver KL, Sengupta S (2001) A plume head and tail in the Bengal basin and Bay of Bengal: Rajmahal and Sylhet Traps with surrounding alkalic volcanism and the Ninetyeast Ridge. EOS Trans Am Geophys Union V12A:0950

Bleeker W (2004) Taking the pulse of planet Earth: a proposal for a new multidisciplinary flagship project in Canadian solid Earth sciences. Geosci Can 31:179–190

Bondre NR, Hart WK, Sheth HC (2006) Geology and geo-chemistry of the Sangamner mafic dike swarm, western Deccanvolcanic province, India: implications for regional stratigraphy. J Geol 114:155–170

Cai K, Sun M, Yuan C, Zhao G, Xiao W, Long X, Wu F (2010) Geochronological and geochemical study of mafic dykes from the northwest Chinese Altai: implications for petrogenesis and tectonic evolution. Gondwana Res 18:638–652

Condie KC (2005) High field strength element ratios in Archean basalts: a window to evolving sources of mantle plumes. Lithos 79:491–504

Condie KC (2018) A planet in transition: The onset of plate tectonics on Earth between 3 and 2 Ga? Geosci Front 9:51–60

Cribb JW, Barton M (1996) Geochemical effects of decoupled fractional crystallization and crustal assimilation. Lithos 37(4):293–307

DePaolo DJ (1981) A neodymium and strontium isotopic study of the Mesozoic calc-alkaline granitic batholiths of the Sierra Nevada and Peninsula Ranges, California. J Geophys Res 86:10470–10488

Ernst RE, Buchan KL, Campbell IH (2005) Frontiers in large igneous province research. Lithos 79:271–297

Ernst RE, Grosfils EB, Mege D (2001) Giant dyke swarms on Earth, Venus, and Mars. Ann. Rev. Earth Planet Sci 29:489–534

Ernst RE, Head JW, Parfitt E, Grosfils E, Wilson L (1995) Giant radiating dyke swarms on Earth and Venus. Earth-Sci Rev 39:1–58

Ernst RE, Srivastava RK, Bleeker W, Hamilton M (2010) Precambrian Large Igneous Provinces (LIPs) and their dyke swarms: new insights from high precision geochronology integrated with paleomagnetism and geochemistry. Precambrian Res 183:vi–xi

Ernst RE, Buchan KL (1997) Giant radiating dyke swarms: their use in identifying pre-Mesozoic large igneous provinces and mantle plumes. In: Large Igneous Provinces: Continental, Oceanic, and Planetary Volcanism, Mahoney J, Coffin M (eds.), Geophy Monograph Series, vol 100. Am Geophy Un, pp 297–333

Esroy Y, Helvaci C (2010) FC–AFC–FCA and mixing modeler: A Microsoft Excel spreadsheet program for modeling geochemical differentiation of magma by crystal fractionation, crustal assimilation and mixing. Comput Geosci 36:383–390

Fitton JG, Saunders AD, Norry MJ, Hardarson BS, Taylor RN (1997) Thermal and chemical structure of the Iceland plume. Earth Planet Sci Lett 153:197–208

Frey FA, McNaughton NJ, Nelson DR, deLaeter JR, Duncan RA (1996) Petrogenesis of the Bunbury basalt, Western Australia:interaction between the Kerguelen plume and Gondwana lithosphere? Earth Planet Sci Lett 144(1–2):163–183

Frey FA, Weis D, Borisova AY, Xu G (2002) Involvement of continental crust in the formation of the cretaceous Kerguelen plateau: new perspectives from ODP leg 120 sites. J Petrol 43:1207–1239

Furman TY, Bryce JG, Karson J, and Iotti A (2004) East African rift system (EARS) plume structure: Insight from quaternary mafic lavas of Turkana, Kenya. J Petrol 45:1069–1088

Gautier I, Weis D, Mennessier JP, Vidal P, Giret A, Loubet M (1990) Petrology and geochemistry of the Kerguelen archipelago basalts (South Indian Ocean): evolution of the mantle sources from ridge to intraplate position. Earth Planet Sci Lett 100:59–76

Ghatak A, Basu AR (2011) Vestiges of the Kerguelen plume in the Sylhet Traps, northeastern India. Earth Planet Sci Lett 308:52–64

Ghatak A, Basu AR (2013) Isotopic and trace element geochemistry of alkalic–mafic–ultramafic–carbonatitic complexes and flood basalts in NE India: Origin in a heterogeneous Kerguelen plume. Geochim Cosmochim Acta 115:46–72

Gudmundsson A (1983) Form and dimensions of dykes in eastern Iceland. Tectonophy 95:295–307

Gudmundsson A (1984) Tectonic aspects of dykes in northwestern Iceland. Jökull 34:81–96

Gudmundsson A (1995) The geometry and growth of dykes. In: Baer G, Heimann A (eds) Physics and chemistry of dykes. Balkema, Rotterdam, pp 23–34

Gudmundsson A, Marinoni LB (2002) Geometry, emplacement and arrest of dykes. Annales Tectoicæ 13:71–92

Halamaa R, Marks M, Brugmann G, Siebela W, Wenzel T, Markl G (2004) Crustal contamination of mafic magmas: evidence from a petrological, geochemical and Sr–Nd–Os–O isotopic study of the Proterozoic Isortoq dike swarm, South Greenland. Lithos 74: 199–232

Halls HC, Fahrig WF (1987) Mafic dyke swarms. Geol. Soc. Canada, Sp. Pap. 34

Hari KR, Swarnkar V, Prasanth MPM (2018) Significance of assimilation and fractional crystallization (AFC) process in the generation of basaltic lava flows from Chhotaudepur area, Deccan Large Igneous Province, NW India. J Earth Sys Sci 127:85

Hoda SQ, Rawat TPS, Krishnamurthy P, Dwivedy KK (1997) Geology and economic resources of the Samchampi alkaline carbonatite complex, Mikir hills, Assam, India. Explora Res At Miner 10:79–86

Hooper PR, Hawkesworth CJ (1993) Isotopic and geochemical constraints on the origin and evolution of the Columbia River Basalt. J Petrol 34:1203–1246

Islam MS, Meshesha D, Shinjo R (2014) Mantle source characterization of Sylhet Traps, northeastern India: A petrological and geochemical study. J Earth Sys Sci 123:1839–1855

James SD, Pearce JA, Oliver RA (1987) The geochemistry of Lower Proterozoic Willyama Complex volcanics, Broken Hill Block, New South Wales. Geol Soc Lond Sp Pub 33:95–408

Janoušek V, Farrow CM, Erban V (2006) Interpretation of Whole-rock Geochemical Data in Igneous Geochemistry: Introducing Geochemical Data Toolkit (GCDkit). J Petrol 47:1255–1259

Jochum KP, Weis U, Schwager B, Stoll B, Wilson SA, Haug GH, Andreae MO, Enzweiler J (2015) Reference Values Following ISO Guidelines for Frequently Requested Rock Reference Materials. Geostand Geoanal Res 40(3):333–350

Jourdan F, Bertrand H, Scharer U, Blichert-Toft J, Feraud J, Kampunzu B (2007) Major and Trace Element and Sr, Nd, Hf, and Pb Isotope Compositions of the Karoo Large Igneous Province, Botswana-Zimbabwe: Lithosphere vs Mantle Plume Contribution. J Petrol 48:1043–1077

Kent RW, Saunders AD, Kempton PD, Ghose NC (eds.) (1997) Rajmahal basalts, Eastern India: mantle sources and melt distribution at a volcanic rifted margin. Geophysical Monograph (AGU), Washington DC, pp 145–182

Kent RW, Pringle MS, Muller RD, Saunders AD, Ghose NC (2002) 40Ar/39Ar geochronology of the Rajmahal basalts, India, and their relationship to the Kerguelen plateau. J Petrol 43:1141–1153

Kumar D, Mamallan R, Dwivedy KK (1996) Carbonatite magmatism in north India. J South Asian Earth Sci 13:145–158

Kumar S, Rino V, Hayasaka Y, Kimura K, Raju S, Terada K, Pathak M (2017) Contribution of Columbia and Gondwana Supercontinent assembly- and growth-related magmatism in the evolution of the Meghalaya Plateau and the Mikir Hills, Northeast India: Constraints from U-Pb SHRIMP zircon geochronology and geochemistry. Lithos 277:356–375

Lassen B, Bridgwater D, Bernstein S, Rosing M (2004) Assimilation and high-pressure fractional crystallization (AFC) recorded by Paleoproterozoic mafic dykes, Southeast Greenland. Lithos 72(1–2):1–18

Le Bas MJ, le Maitre RW, Streckeisen A, Zanettin B (1986) A Chemical Classification of Volcanic Rocks Based on the Total Alkali-Silica Diagram. Journal of Petrology 27(3):745–750

Lofgren GE, Donaldson CH (1975) Curved branching crystals and differentiation in comb-layered rocks. Contrib Mineral Petrol 49:309–319

Mahoney JJ, Jones WB, Frey FA, Salters VJM, Pyle DG, Davies HL (1995) Geochemical characteristics of lavas from broken ridge, the Naturaliste plateau and southernmost Kerguelen plateau: cretaceous plateau volcanism in the Southeast Indian Ocean. Chem Geol 120(3–4):315–345

Mallikharjuna Rao J (2002) Petrology and geochemistry of dolerite dykes, West Garo Hills Meghalaya – a preliminary study. Gondwana Res 5:884–888

Mattielli N, Weis D, Blichert Toft J, Albarede F (2002) Hf isotope evidence for a Miocene change in the Kerguelen mantle plume composition. J Petrol 43:1327–1339

McHone JG, Anderson DL, Beutel EK, Fialko YA (2005) Giant dykes, rifts, flood basalts, and plate tectonics: a contention of mantle models. In: Foulger GR, Natland JH, Presnall DC, Anderson DL (eds) Plates, plumes and paradigms. Geol Soc Am Sp Pap 38:401–420

Meschede M (1986) A method of discriminating between different types of mid-oceanic ridge basalts and continental tholeiites with Nb-Zr-Y diagram. Chem Geol 56:207–218

Morimoto N (1988) Nomenclatures of pyroxenes. Am Mineral 73:1123–1133

Mungall JE (2007) Crustal Contamination of Picritic Magmas During Transport Through Dikes: the Expo Intrusive Suite, Cape Smith Fold Belt, New Quebec. J Petrol 48(5):1021–1039

Nag S, Sengupta SK, Gaur RK, Absar A (1999) Alkaline rocks of Samchampi-Samteran, District Karbi-Anglong, Assam, India. Proc Indian Acad Sci (Earth Planet Sci) 108:33–48

Neal CR, Mahoney JJ, Chazey WJ III (2002) Mantle sources and the highly variable role of continental lithosphere in basalt petrogenesis of the Kerguelen plateau and broken ridge LIP: results from ODP leg 183. J Petrol 43:1177–1205

Neumann E-R, Svensen H, Galerne CY, Planke S (2011) Multistage evolution of dolerites in the Karoo large igneous province, Central South Africa. J Petrol 52:959–984

Pantulu G, Macdougall JD, Gopalan K, Krishnamurthy P (1992) Isotopic and chemical compositions of Sylhet Traps basalts: links to the Rajmahal Traps and Kerguelen hotspot. Trans Am Geophys Union 72:328

Parker AJ, Rickwood PC, Tucker DH (eds) (1990) Mafic dykes and emplacement mechanisms. Balkema, Rotterdam

Pearce JA, Norry MJ (1979) Petrogenetic implications of Ti, Zr, Y, and Nb variations in volcanic rock. Contrib Mineral Petrol 69:33–47

Putirka KD (2008) Thermometers and barometers for volcanic systems. Rev Mineral Petrol 69:61–120

Ray JS, Pattanayak SK, Pande K (2005) Rapid emplacement of the Kerguelen Plume related Sylhet Traps, eastern India: Evidence from $^{40}Ar–^{39}Ar$ geochronology. Geophys Res Lett 32:1–4

Rudnick RL, Fountain DM (1995) Nature and composition of the continental crust: lower crustal perspective. Rev Geophys 33:267–309

Rudnick RL, Gao S (2003) Composition of the continental crust, in Holland HD. In: Turekin KK (ed) Treatise on geochemistry. Elsevier, Oxford, pp 1–64

Sen B, Pal T (2019) P-type pahoehoe lava in the eastern parts of Sylhet Traps and its implication on mechanism of flow emplacement. Indian J Geosci 73:67–74

Srivastava RK, Heaman LM, Sinha AK, Shihua S (2005) Emplacement age and isotope geochemistry of Sung Valley alkaline–carbonatite complex, Shillong Plateau, northeastern India: Implications for primary carbonate melt and genesis of the associated silicate rocks. Lithos 81:33–54

Srivastava RK, Kumar S, Sinha AK, Chalapathi Rao NV (2014) Petrology and geochemistry of high-titanium and low-titanium mafic dykes from the Damodar valley, Chhotanagpur Gneissic Terrain, eastern India and their relation to Cretaceous mantle plume(s). J Asian Earth Sci 84:34–50

Srivastava RK, Sinha AK (2004) Geochemistry and petrogenesis of early Cretaceous sub-alkaline mafic dykes from Swangkre-Rongmil, East Garo Hills, Shillong plateau, Northeast India. Earth Planet Sci (Proc Indian Acad Sci) 113:683–697

Srivastava RK, Sinha AK, Kumar S (2012) Geochemical characteristics of Mesoproterozoic metabasite dykes from the Chotanagpur Gneissic Terrain, eastern India: implications for their emplacement in a plate margin tectonic environment. J Earth Sys Sci 121:509–523

Storey M, Kent RW, Saunders AD, Hergt J, Salters VJM, Whitechurch H, Sevigny JH, Thirlwall MF, Leat P, Ghose NC, Gifford M (1992) Lower cretaceous volcanic rocks on continental margins and their relationship to the Kerguelen plateaus. In: Wise SW, Schlich R (eds) Proceedings of the ocean drilling program:scientific results, vol 120. Ocean Drilling Program, College Station, TX, pp 33–53

Sun S-S, McDonough WF (1989) Chemical and isotopic systematics of oceanic basalts: implications for mantle composition and processes. In: Saunders AD, Norry MJ (eds) Magmatism in Ocean Basins. Geol Soc Sp Pub, London, pp 313–345

Talukdar SC, Murthy MVN (1971) The Sylhet Traps, their tectonic history, and their bearing on problems of Indian Flood Basalt Provinces. Bull Volcanol 35:602–618

Talukdar SC (1967) Rhyolite and alkali basalt from the Sylhet Traps, Khasi Hills, Assam. Curr Sci 9:238–239

Tatsumi Y, Eggins SM (1995) Subduction Zone Magmatism. Blackwell, Oxford

Vanderkluysen L, Mahoney JJ, Hooper PR, Sheth HC, Ray R (2011) The Feeder System of the Deccan Traps (India): Insights from Dike Geochemistry. J Petrol 52:315–343

Veena K, Pandey BK, Krishnamurthy P, Gupta JN (1998) Sr and Nd isotopic systematics of the carbonatites of Sung Valley, Meghalaya, Northeast India: Implications for contemporary plume-related mantle source characteristics. J Petrol 39:1875–1884

Weaver BL (1991) The origin of ocean island basalt end member composition: trace element and isotopic constrain. Earth Planet Sci Lett 104:381–397

Weaver BL, Turney J (1984) Empirical approach to estimating composition of continental crust. Nature 310:575–577

Wilson M (1989) Igneous Petrogenesis-A Global Tectonic Approach. Springer, Dordrecht

Winchester JA, Floyd PA (1977) Geochemical discrimination of different magma series and their differentiation products using immobile elements. Chem Geol 20:325–343

Winter JD (2014) Principles of Igneous and Metamorphic Petrology (2nd Ed.) Pearson Education Limited

Xia L, Li X (2019) Basalt geochemistry as a diagnostic indicator of tectonic setting. Gondwana Res 65:43–67

Cao X, Gao X, Lü X, Qin Q, Liu S, Chen C, Guo R, Zhang B, Hu Q (2011) Sm–Nd geochronology and geochemistry of a Neoproterozoic gabbro in the Kuluketageblock, North-Western China. Int Geol Rev:1–15. https://doi.org/10.1080/00206814.2011.639946

Wang P, Glover L (1992) A tectonics test of the most commonly used geochemical discriminant diagrams and patterns. Earth Sci Rev 33(2):111–131

Xie X, Yan M, Li L, Shen H (1985) Geochemical Reference Samples, Drainage Sediment GSD 1–8 from China. Geostand Newslett 9(1): 83–159

Yin A, Dubey CS, Webb AAG, Kelty TK, Grove M, Gehrels GE, Burgess WP (2010) Geologic correlation of the Himalayan orogen and Indian craton: Part 1. Structural geology, U-Pb zircon geochronology, and tectonic evolution of the Shillong Plateau and its neighboring regions in NE India. Geol Soc Am Bull 122:336–359

Zhao JH, Zhou MF (2007) Geochemistry of Neoproterozoic mafic intrusions in the Panzhihua district (Sichuan Province, SW China): implications for subduction-related metasomatism in the upper mantle. Precambrian Res 152:27–47